

1 **Review: Large-Eddy Simulation of the Atmospheric**
2 **Boundary Layer**

3 **Rob Stoll Jeremy A. Gibbs Scott T. Salesky,**
4 **William Anderson, Marc Calaf**

5
6 Received: March 2020

7 **Abstract** Over the last 50 years the large-eddy simulation (LES) technique has de-
8 veloped into one of the most prominent numerical tools used to study transport pro-
9 cesses in the atmospheric boundary layer (ABL). This review examines development
10 of the technique as a tool for ABL research, integration with state-of-the-art scientific
11 computing resources, and some key application areas. Analysis of the published liter-
12 ature indicates that LES research across a broad range of applications accelerated
13 starting in about 1990. From that point in time, robust research using LES developed
14 in several different application areas and based on a review of the papers published
15 in this journal, we identify seven major areas of intensive ABL LES research: con-
16 vective boundary layers, stable boundary layers, transitional boundary layers, plant
17 canopy flows, urban meteorology and dispersion, surface heterogeneity, and the test-
18 ing and development of subgrid scale (SGS) models. The review begins with a general
19 overview of LES and then proceeds to examine the SGS models developed for use in
20 ABL LES. After this overview of the technique itself, we review the specific model
21 developments tailored to the identified application areas and the scientific advance-
22 ments realized using the LES technique in each area. We conclude by examining the

R. Stoll (Correspondence)
University of Utah, Department of Mechanical Engineering, Salt Lake City, UT USA 84112
E-mail: rstoll@eng.utah.edu

J. A. Gibbs
NOAA/OAR National Severe Storms Laboratory, Norman, Oklahoma
E-mail: jeremy.gibbs@noaa.gov

S. T. Salesky
School of Meteorology, University of Oklahoma, Norman, Oklahoma 73072, USA
E-mail: salesky@ou.edu

W. Anderson
The University of Texas at Dallas, Department of Mechanical Engineering
E-mail: wca140030@utdallas.edu

M. Calaf
University of Utah, Department of Mechanical Engineering, Salt Lake City, UT USA 84112
E-mail: marc.calaf@utah.edu

23 computational trends in published ABL LES research and identify some resource un-
 24 derutilization. Future directions and research needs are identified from a synthesis of
 25 the reviewed literature.

26 **Keywords** numerical simulation convective boundary layer stable boundary
 27 layer plant canopy urban canopy layer surface heterogeneity subgrid scale
 28 model

29 1 Introduction

30 A central component of atmospheric boundary layer (ABL) research is the study of
 31 turbulent fluxes of mass, momentum, heat, and pollutants (Garratt 1992). These fluxes
 32 govern land-atmosphere interactions critical to a wide variety of applications includ-
 33 ing weather and climate prediction (Teixeira et al. 2008; Holtslag et al. 2013), agricul-
 34 tural water use and productivity (Brutsaert 1982), the dispersion of pollen and spores
 35 in natural and agricultural systems (Mahaffee and Stoll 2016), urban-air quality and
 36 energy use (Pardyjak and Stoll 2017), and many others. Because of their role in a wide
 37 range of environmental processes, researchers have developed an array of methods to
 38 probe turbulence in the ABL, each with its own strengths and weaknesses (LeMone
 39 et al. 2019).

40 One of the most prominent numerical methods used to examine turbulence in the
 41 ABL is the large-eddy simulation (LES) technique. In LES, the conservation equations
 42 of mass, momentum, heat, and scalars are filtered with a characteristic spatial filter of
 43 width Δ (Lesieur et al. 2005; Sagaut 2006; Wyngaard 2010), which in the ABL with
 44 the assumptions of a Boussinesq fluid subject to horizontal Coriolis forces results in

$$45 \quad \frac{\partial \tilde{u}_{i\psi}}{\partial x_{i\psi}} = 0 \quad (1)$$

$$46 \quad \frac{\partial \tilde{u}_{i\psi}}{\partial t\psi} + \tilde{u}_{j\psi} \frac{\partial \tilde{u}_{i\psi}}{\partial x_{j\psi}} = -\frac{1}{\rho} \frac{\partial \tilde{p}\psi}{\partial x_{i\psi}} - f_c \epsilon_{ij3} u_{j\psi} - \delta_{i3} \frac{\tilde{\theta}_v - \langle \tilde{\theta}_v \rangle}{\theta_0} - \frac{\partial \tau_{ij\psi}}{\partial x_{j\psi}} + F_{i\psi} \quad (2)$$

$$47 \quad \frac{\partial \tilde{\theta}\psi}{\partial t\psi} + \tilde{u}_{i\psi} \frac{\partial \tilde{\theta}\psi}{\partial x_{i\psi}} = -\frac{\partial q_{i\psi}}{\partial x_{i\psi}} + Q\psi \quad (3)$$

48 where the $\tilde{\dots}$ indicates a quantity that is filtered with a low-pass convolution filter
 49 (Sagaut 2006), $u_{i\psi}$ is the velocity in the i^{th} direction with $i\psi = 1-3$ representing the
 50 streamwise (u), spanwise (v), and surface normal (w) velocity components, respec-
 51 tively, $x_{i\psi}$ is the spatial coordinate corresponding to directions of the $\tilde{u}(x_i, t)$, $\tilde{v}(x_i, t)$,
 52 and $\tilde{w}(x_i, t)$ velocity components, p is the dynamic pressure, ρ is air density, f_c is the
 53 Coriolis frequency at a pre-defined latitude, $\theta(x_i, t)$ represents the potential tempera-
 54 ture for heat or a generic scalar concentration for the transport of moisture, pollutants,
 55 or other transported scalars, θ_v is the virtual potential temperature, θ_0 is a reference
 56 virtual potential temperature, averaging over a region of interest is denoted by angle
 57 brackets, $\langle \dots \rangle_{a\psi}$ where a , when present, is the dimension over which averaging is per-
 58 formed, $Q\psi$ is a volumetric source or sink of heat or scalar, $\tau_{ij\psi}$ and $q_{i\psi}$ represent the
 59 contribution of subfilter scale (SFS) stress and flux, respectively, and $F_{i\psi}$ represents

60 a generic body force used to represent the momentum-depleting influence of non-
61 boundary porous or solid objects in the flow (e.g., trees or buildings using a porous
62 flow or immersed boundary method). In equations 2 and 3, viscous effects have been
63 neglected. This is a standard assumption in LES of the ABL where the Reynolds num-
64 ber is typically very large.

65 The LES technique and its use in atmospheric science has origins in the work of
66 Smagorinsky (1963) and Lilly (1967). Since that time, its use has expanded consider-
67 ably and it is now one of the dominant numerical techniques used to examine turbulent
68 fluxes in a wide range of atmospheric and engineering applications. This is borne out
69 by examining the percentage of total annual articles published in three representative
70 journals in which LES is a notable component. The considered journals include one
71 focused on ABL research (*Boundary-Layer Meteorology*, BLM), one focused on gen-
72 eral atmospheric science research (*Journal of the Atmospheric Sciences*, JAS), and
73 one that publishes exemplary research in all classes of fluid mechanics (*Journal of*
74 *Fluid Mechanics*, JFM). This review focuses on ABL LES and to that end, JAS and
75 JFM were chosen to provide context for trends observed in BLM, which we use as a
76 proxy for general ABL research due to its relatively specific focus. Articles were in-
77 cluded if they referenced LES in their keywords, title, or abstract. This does not mean
78 that all articles are numerical in nature, only that the LES technique plays a prominent
79 role in the presented research.

80 The most obvious trend shown in Fig. 1 is the upward trajectory in the number of
81 articles mentioning LES in all three journals since 1990. While a definitive reason for
82 the timing of this inflection is difficult to surmise, the early 1990s saw several advances
83 in computational science that likely contributed to the rapid spread of LES. These in-
84 clude the first massively-parallel and widely-available computing clusters (Castagnera
85 et al. 1994), the standardization of the message passing interface (MPI, Gropp et al.
86 1996), and the introduction of the Pentium® line of microprocessors (Colwell 2019).
87 A second observation is the clear importance of LES in ABL research. Starting from
88 2006, almost 20% of all articles published in BLM featured LES with a maximum
89 of 39% in 2017. Just as striking is that although JFM and JAS both currently publish
90 approximately six times more articles per year than BLM, BLM publishes a nearly
91 equal amount of LES articles as JAS and on the order of half that of JFM.

92 LES articles published in BLM cover a wide range of topics (Fig. 2). The word
93 cloud consists of keywords from all identified LES papers (as described above) with a
94 minimum of four mentions. General keywords that appear in many articles but are not
95 related to the LES topic of inquiry are excluded for clarity (e.g., atmospheric bound-
96 ary layer, large-eddy simulation). While the breadth of topics is extensive, a few re-
97 search areas stand out and these areas have been chosen in this review for detailed
98 analysis. The most prominent is one of the first ABL topics to be explored (Deardorff
99 1972a), the convective boundary layer (CBL) and its closely related topics (entrain-
100 ment, mixed layer, convection). A clear second, is research on the stable boundary
101 layer (SBL) and stable stratification. After this, topic areas are still identifiable but
102 the author self-identified topic names become less uniform. The areas we identified
103 include flow in and around plant canopies, dispersion and flow in urban canopies, and
104 heterogeneity and complex terrain. We also find that many articles study the diurnal
105 variation of the ABL and therefore, we explore transitional boundary layers.

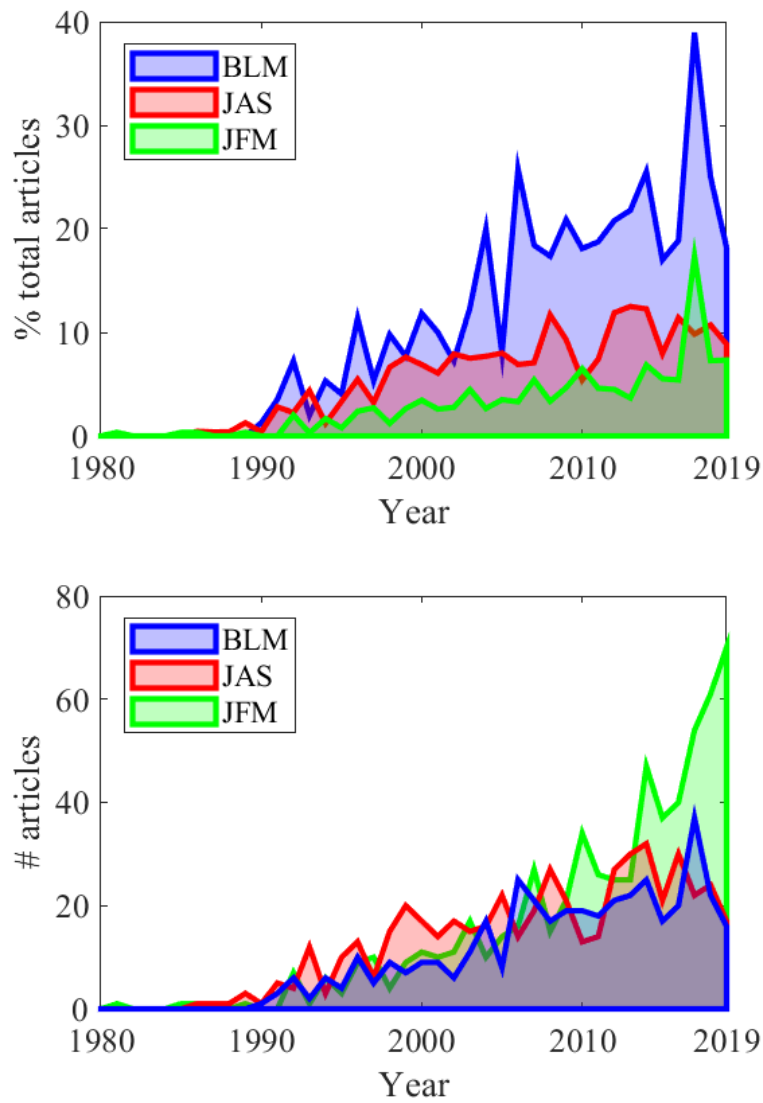


Fig. 1 LES articles published in BLM (blue), JAS (red), and JFM (green) since 1980. The top panel is the percentage of total annual published articles, and the bottom panel is the total number of published articles, in which LES was a prominent component.

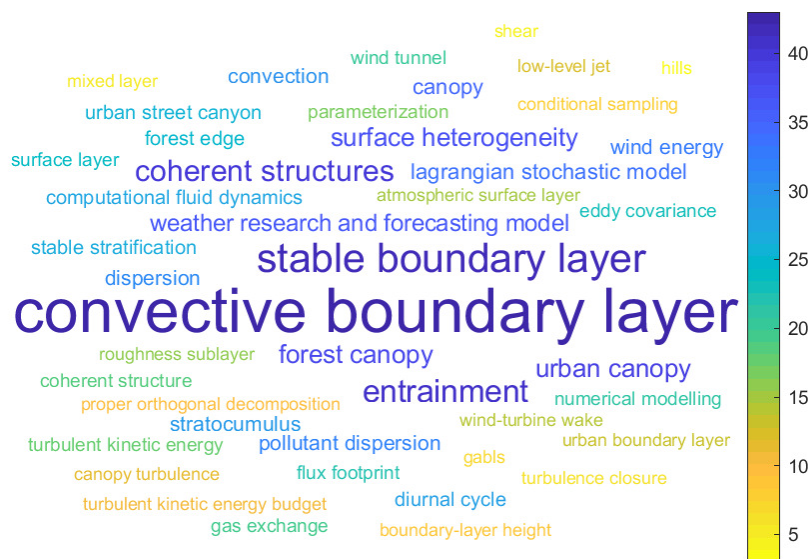


Fig. 2 Word cloud of keywords from LES articles in BLM. The color and relative size of each keyword indicates the number of instances of its usage. Keywords mentioned fewer than four times are excluded.

106 Some areas of research are conspicuously missing, e.g., LES of cloud topped
 107 boundary layers. Performing LES of cloud topped boundary layers entails modelling
 108 challenges related to the representation of cloud microphysics and strong stratifica-
 109 tion (Yamaguchi and Randall 2012; Mellado 2017) that are somewhat unique. The
 110 cloud modelling community has a robust history of simulation intercomparison stud-
 111 ies and interested readers are directed to those for detailed descriptions of LES of
 112 cloudy boundary layers (e.g., Stevens et al. 2005; Ackerman et al. 2009). The selected
 113 research areas reflect the focus on BLM and topics that are prominent in it. Other ar-
 114 eas, for example *a priori* studies of LES SFS models which have been critical in the
 115 development of LES, are not included for brevity. A review of recent developments
 116 in cloud topped boundary layers, *a priori* studies, and other topics not covered here
 117 can be found in LeMone et al. (2019). In addition to the ABL application areas dis-
 118 cussed above, we start our review with an examination of the development of the LES
 119 technique with an emphasis on the history of SFS model evolution.

120 2 LES technique and SFS model development

121 The LES technique was first introduced in Smagorinsky (1963), expounded upon
 122 and formalized by Lilly (1967), and implemented by Deardorff (1970a, 1972a, 1973,
 123 1980). Interestingly, the term “large-eddy simulation” was never used in these seminal

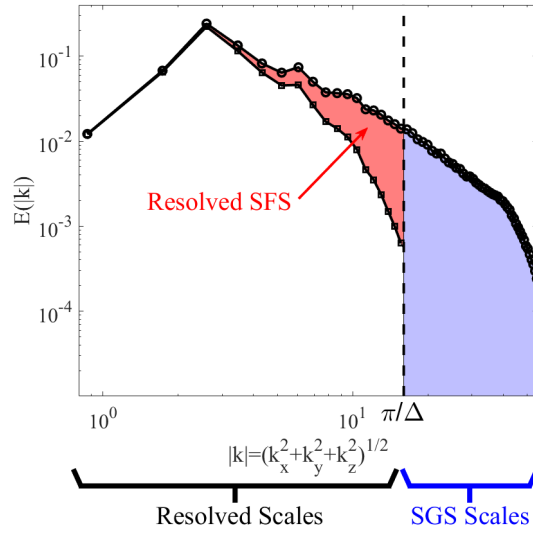


Fig. 3 Illustration of the difference between SFS and SGS using a three-dimensional velocity spectrum obtained from the isotropic turbulence direct numerical simulations of Lu et al. (2008) as an example flow (open circles) and a LES convolution filter with a Gaussian filter kernel (open squares). The red-filled region indicates resolved SFS and the blue-filled region indicates scales that are subgrid.

124 works; it was apparently coined in 1973 by W. C. Reynolds at the Center for Turbu-
 125 lence Research, Stanford University (Moin and Homsy 2017), while Leonard (1974)
 126 was the first to use it in published form (Lilly 2000). The name is derived from the
 127 conceptual underpinnings of the technique, which represents a compromise in bal-
 128 ancing physical realizability with computational burden. With LES, a filter is applied
 129 to the conservation equations at Δ in order to decompose the flow field into large
 130 energy-containing scales and presumably universal small scales. In *physical* LES, the
 131 large scales of the flow (i.e., large eddies) are computed explicitly on the numerical
 132 mesh, while the effects of the small scales are modeled (Pope 2004). Although strictly
 133 numerical approaches are also possible (*numerical* LES), this paper will focus on ap-
 134 plications of *physical* LES to the ABL (see Grinstein et al. 2007 for background and
 135 applications of *numerical* LES).

136 Before continuing, it is important in this context to distinguish between SFS and
 137 subgrid-scale (SGS), despite their colloquial conflation. The latter refers to scales that
 138 fall below the grid spacing increment and is often used when the numerical grid spac-
 139 ing acts as the filter width in the LES conservation equations, while the former is
 140 meant to describe motions whose scales fall below the width of any explicit filter
 141 operation. In other words, SGS motions are always unresolved on the computational
 142 mesh, while SFS motions may be partially resolved (Fig. 3). Please note that the pre-
 143 sented data is used to demonstrate conceptual aspects of filtering and spectral density;
 144 ABL turbulence is additionally affected by land-surface normal heterogeneity.

145 When a filter is applied to the conservation equations, the terms $\widetilde{u_i u_{j\psi}}$ and $\widetilde{u_i \theta_{j\psi}}$ ap-
 146 pear in the resulting expressions for momentum and heat/scalars, respectively. These
 147 terms are problematic because they represent the filtered product of two non-filtered
 148 variables. One does not have knowledge of these variables and thus the terms can-
 149 not be solved *a priori*. Leonard (1974) decomposed and filtered the nonlinear term
 150 in the momentum equation to obtain $\tau_{ij\psi} = L_{ij\psi} + C_{ij\psi} + R_{ij\psi} = \widetilde{u_i u_{j\psi}} - \widetilde{u_i} \widetilde{u_{j\psi}}$. Here,
 151 $C_{ij\psi} = \widetilde{u_i u'_{j\psi}} + \widetilde{u'_j u_{i\psi}}$ describes the interaction between resolved and SFSs, $R_{ij\psi} = \widetilde{u'_i u'_{j\psi}}$ is
 152 the SFS “Reynolds” stress, $L_{ij\psi} = \widetilde{u_i} \widetilde{u_{j\psi}} - \widetilde{u_i} \widetilde{u_{j\psi}}$ is the so-called Leonard stress, which
 153 describes the interaction among the smallest resolved scales, and the prime (*′*) de-
 154 notes deviation from the filtered value. If the filter is a Reynolds operator, then $C_{ij\psi}$
 155 and $L_{ij\psi}$ disappear and $\tau_{ij\psi} = \widetilde{u'_i u'_{j\psi}}$. A similar procedure is applied for scalars.

156 Substituting these expressions into the filtered form of the conservation equations
 157 yields Eqs. (2) and (3), respectively. However, the SFS stress $\tau_{ij\psi}$ and SFS flux $q_{i\psi}$ are
 158 unknown quantities and thus the equations are not closed (the so-called turbulence
 159 “closure problem”). The goal of LES is often to generate realistic statistical proper-
 160 ties of a considered turbulent flow. To that end, it is a necessary but not sufficient
 161 condition for an SFS model to provide the correct distributions of mean energy dis-
 162 sipation and stress in order to properly capture flow statistics (Meneveau and Katz
 163 2000). Accordingly, a primary challenge in LES is modeling $\tau_{ij\psi}$ and q_i . Much of the
 164 early work developing the LES technique focused on these two terms, but it must
 165 be recognized that the development and performance of LES SFS models cannot be
 166 disentangled from the numerical representation and solution methodology used for
 167 Eqs. 1-3. The type of filter used to separate resolved and SFSs (Geurts 2003; Wyn-
 168 gaard 2010), the chosen spatial discretization scheme (see Giacomini and Giometto
 169 2020, for a review of techniques), and the chosen time integration scheme (Gibbs and
 170 Fedorovich 2014b) all have significant impacts on the representation of turbulence
 171 and the effective resolution of a given numerical code (Moeng and Wyngaard 1988;
 172 Gibbs and Fedorovich 2014a). The subject of numerical discretization is a wide rang-
 173 ing one that has a critical role in LES. In this section we give a brief overview of the
 174 historical LES technique and SFS model development, from Smagorinsky to modern
 175 day with a focus on the physical aspects. For more details on the numerical aspects,
 176 we refer interested readers to the aforementioned references.

177 2.1 Eddy-viscosity models

178 Eddy-viscosity (EV) models are the most widely used class of SFS models and are
 179 mathematically analogous to the molecular properties of Newtonian fluids. For a constant-
 180 property Newtonian fluid, the stress tensor is linearly related to the mean shear through
 181 the molecular viscosity of the fluid (Pope 2000). Similarly, EV models assume that
 182 the deviatoric part of the Reynolds stress is linearly related to the mean rate-of-strain

183 of a flow through an eddy viscosity:

$$184 \quad \tau_{ij\psi} = -2\nu_T \tilde{S}_{ij\psi} \quad (4)$$

$$185 \quad q_{i\psi} = -\nu_{\theta\psi} \frac{\partial \tilde{\theta}}{\partial x_i}, \quad (5)$$

186 where $\nu_{T\psi}$ is the eddy viscosity, $\tilde{S}_{ij\psi} = 0.5 (\partial \tilde{u}_i / \partial x_j + \partial \tilde{u}_j / \partial x_i)$ is the filtered strain
187 rate tensor, and $\nu_{\theta\psi}$ is the eddy diffusivity.

188 Examination of even basic turbulent flows has shown that there is no general phys-
189 ical validity to this assumption (Pope 2000). Additionally, EV models extract energy
190 from the simulation's resolved scales, mimicking the average energy transfer in the
191 turbulent cascade, making them purely dissipative and thus they only represent the
192 statistically averaged flow of energy and not the combined instantaneous forward scatter
193 and backscatter observed over large portions of the flow in, e.g., DNS of channel
194 flow (Piomelli et al. 1991). Despite these drawbacks, the EV model has proven to be
195 a reasonable approach across a range of flow scenarios.

196 Smagorinsky (1963) was the first to introduce an EV model in an attempt to
197 parametrize the effects of three-dimensional small scale motions in simulations of
198 quasi-two-dimensional synoptic-scale atmospheric circulation. The chosen EV re-
199 lated local variables to flow features at a length scale equal to the numerical grid
200 spacing (Métais 1998). The Smagorinsky model was based on work from colleagues
201 in von Neumann's group at Princeton, in which one-dimensional acoustic shocks were
202 smoothed through the use of an artificial viscosity that was proportional to the local
203 gradient of the flow field and the square of the spacing between data points (Lilly
204 2000). Although Smagorinsky's model is overly dissipative of large-scale atmospheric
205 motions, it remains popular. More importantly, it served as a catalyst for future de-
206 velopment of the LES technique and SFS models. Smagorinsky (1963) proposed the
207 following model, which is based on the mixing-length theory of Prandtl (1925):

$$208 \quad \tau_{ij\psi} = -2(C_S \Delta)^2 |\tilde{S}| \tilde{S}_{ij\psi} \quad (6)$$

209 where $\Delta = (\Delta_x \Delta_y \Delta_z)^{\frac{1}{3}}$ is a length scale based on the grid spacing increments in
210 each direction, $C_{S\psi}$ is a constant, and $|\tilde{S}| = \sqrt{2\tilde{S}_{ij}\tilde{S}_{ij}}$ can be considered as a rep-
211 resentative velocity scale for transport at SFSs. Lilly (1967) was the first to derive a
212 filter-dependent, grid-increment-independent expression for C_S . It was shown in *op.*
213 *cit.* that $C_{S\psi} \approx 0.17$ for a spectral cutoff filter under the assumption of Kolmogorov
214 turbulence (Kolmogorov et al. 1991, K-41). The combined efforts between these two
215 scientists explains why Eq. 6 is often referred to as the Smagorinsky-Lilly model.

216 Deardorff (1970a) first implemented the Smagorinsky-Lilly model in a numerical
217 simulation of plane Poiseuille flow to study turbulence properties at large Reynolds
218 numbers. The modest numerical mesh of $24 \times 14 \times 20$ points was a limitation of
219 memory availability in the CDC 6600 Supercomputer at the *National Center for Atmo-*
220 *spheric Research*. Deardorff tested several values of $C_{S\psi}$ and found that Lilly's value of
221 0.17 resulted in excessively damped small-scale motions and subsequently settled on
222 $C_{S\psi} = 0.10$. Results, as compared with laboratory measurements, were deemed "good

to marginal". In follow-up studies using larger numerical grids of up to $40 \times 40 \times 20$ points, Deardorff (1971, 1972a) reported that $C_{S\psi}$ should be changed to 0.21 (0.13) for unstably (neutrally) stratified flows. The modification was justified by noting that large-scale mean flow derived from, e.g. a constant pressure gradient, should be removed from the computation of the SGS eddy coefficient. Despite the additional information gleaned from the adjustment to C_S , Deardorff noted the limitations of the Smagorinsky-Lilly model in the presence of stably-stratified regions.

Deardorff (1980, D80) used an alternative form for the EV as an approach to improve the representation of stratification without resorting to solving prognostic equations for τ_{ij} . The EV was taken as $v_{T\psi} = C_1 \ell \sqrt{E}$, where $C_1 = 0.1$ and $\ell = \Delta(\partial \tilde{b} / \partial x_3 \leq 0), \min[\Delta, 0.5\sqrt{E}/N\psi](\partial \tilde{b} / \partial x_3 > \psi 0)$ is the turbulence length scale, in which $b\psi$ is buoyancy and $N\psi$ is the Brunt-Väisälä frequency. The SGS kinetic energy $E\psi$ (used in the representative velocity scale) and was found using the following parameterized transport equation:

$$\frac{\partial E\psi}{\partial t\psi} = -\frac{\partial \tilde{u}_j E\psi}{\partial x_{j\psi}} + 2\nu_T \tilde{S}_{ij} \tilde{S}_{ij\psi} - \nu_{\theta\psi} \frac{\partial \tilde{b}\psi}{\partial z\psi} + \frac{\partial \psi}{\partial x_{j\psi}} 2\nu_{T\psi} \frac{\partial E\psi}{\partial x_{j\psi}} - \epsilon.\psi \quad (7)$$

The eddy diffusivity and SGS turbulence kinetic energy (TKE) dissipation were modeled, respectively, as:

$$\nu_{\theta\psi} = \left(1 + 2\frac{\ell}{\Delta}\right) \nu_{T\psi} \quad \text{and} \quad \epsilon\psi = C_e \frac{E^{3/2}}{\ell},$$

where $C\psi = \xi_{\psi}(0.19 + 0.51\ell/\Delta)$ and ξ_{ψ} is an optional wall-correction function. The modeled dissipation rate is included to ensure that the mean energy transfer from the resolved scales is balanced in accordance with K-41. While the model is commonly credited to Deardorff, it is similar to one proposed by Schumann (1975) for the isotropic part of a two-part EV model. In fact, Sullivan et al. (1994) proposed a two-part EV model based, in part, on Schumann (1975) and D80 that added mean-shear contributions to the SGS TKE transport equation to improve results near the lower boundary. The D80 model also served as the SGS model in the first pseudo-spectral LES of the ABL (Moeng 1984) and models based on D80 remain popular due to the ability to include SGS transport or energy drain effects as extra parameters in the SGS kinetic energy transport equation. Recently, Gibbs and Fedorovich (2016, GF16) revisited the D80 model and proposed removing the stability-dependent length scale and near-wall enhancement of dissipation if the numerical grid spacing is adequately fine, and introduced a new stability-dependent formulation for $\nu_{\theta\psi}$ based on the Richardson number (Ri). The GF16 model better captured near-surface predictions of TKE, stability, and sensible heat flux.

2.2 Alternatives to eddy-viscosity models

Additional methods were motivated by the EV approach pioneered by Smagorinsky. To address deficiencies in early applications of Eq. 6, Deardorff (1973) introduced a

260 2nd-order model which required closure of the SFS transport equations. The pressure-
 261 velocity correlations were ignored while the triple correlation, pressure-strain correla-
 262 tion, and dissipation were modeled as functions of SGS kinetic energy E_{ψ} (which
 263 was taken as the square of the relevant velocity scale). While results using the new
 264 transport model indicated better representation of fluxes than those predicted by the
 265 Smagorinsky-Lilly model, the simulations were 2.5 times more expensive computa-
 266 tionally and the model was still subject to the limitations of the EV closure paradigm.

267 Another set of alternative models use the idea of scale-similarity, which assumes
 268 that the statistical structure of tensors constructed on the basis of the SFSs is simi-
 269 lar to that of the equivalent tensors evaluated using the smallest resolved scales. The
 270 idea (loosely motivated by Leonard 1974) is that the unresolved scales and small-
 271 est resolved scales have a common history through interactions with the largest re-
 272 solved scales, and that some structures appear in all three bands leading to strong
 273 correlations among each level of decomposition. Bardina et al. (1980) proposed the
 274 first scale-similarity model, which was later generalized by Liu et al. (1994). Scale-
 275 similarity models were quite computationally expensive due to the use of multiple
 276 explicit filtering operations. This limitation motivated the development of nonlinear
 277 models, which approximate $\tilde{u}_{i\psi}$ by a Taylor series expansion around the “true” mean
 278 at a point. This procedure is far less computationally expensive since no additional
 279 explicit filtering operations are required.

280 Although similarity and nonlinear models exhibit a high level of correlation in *a*
 281 *priori* tests with measured values of τ_{ij} , they underestimate the average dissipation
 282 and are numerically unstable. As a result, they are combined with an EV model to
 283 provide the proper level of dissipation. In ABL research, mixed models have been
 284 implemented using the explicit filtering and reconstruction method described in Chow
 285 et al. (2005) and Mirocha et al. (2010).

286 A less-known alternative approach used in ABL research is the stochastic model
 287 in which stochastic subgrid stress variations are added to a base SGS model. In Mason
 288 and Thomson (1992), these variations were added to the Smagorinsky-Lilly model.
 289 Results indicated an energy backscatter rate slightly larger than the dissipation rate,
 290 which would otherwise be disallowed in the Smagorinsky-Lilly model. Accordingly,
 291 there was a substantial improvement in the near-wall region of the flow and a better
 292 logarithmic profile.

293 2.3 Dynamic models

294 All of the presented models to this point include at least one model coefficient that
 295 must be prescribed based on theoretical considerations (e.g., isotropy), empirical data,
 296 or chosen *ad hoc* to recover the “correct” *a posteriori* results from simulations. Ger-
 297 mano et al. (1991) pioneered a procedure to dynamically calculate these unknown
 298 model coefficients, leading to the so-called dynamic model. An analogous procedure
 299 was first applied to scalars and compressible flows by Moin et al. (1991). In the dy-
 300 namic procedure, a second filter (the test filter; denoted by $\overline{\overline{\cdot}}$) is applied to Eq. 2 at a

301 larger scale (e.g., 2Δ), which results in the Germano identity:

$$302 \quad L_{ij\psi} = T_{ij\psi} - \overline{\tau_{ij\psi}} = \overline{\tilde{u}_i \tilde{u}_j \psi} - \overline{\tilde{u}_i} \overline{\tilde{u}_j}, \quad (8)$$

303 where $T_{ij\psi}$ is the SFS stress at the 2Δ level. If it is assumed the same SFS model
 304 can be applied for the stress at Δ and 2Δ (e.g., 2Δ) it can be exploited to derive
 305 model coefficients for any base model. Lilly (1992) applied the dynamic procedure
 306 to the Smagorinsky-Lilly model. By minimizing the associated square error of this
 307 combination, Lilly arrived at the following expression for the model coefficient

$$308 \quad C_{S\psi}^2 = \frac{L_{ij} M_{ij}}{M_{ij} M_{ij\psi}},$$

309 where

$$310 \quad M_{ij\psi} = 2\Delta^2 \left[\overline{|\tilde{S}| \tilde{S}_{ij\psi}^2} - 2 \overline{|\tilde{S}\psi| \tilde{S}_{ij\psi}} \right]. \psi$$

311 This procedure is not limited to the Lilly-Smagorinsky model and can be applied
 312 to other base SFS models with one (e.g., Wong and Lilly 1994) or more model co-
 313 efficients (e.g., Anderson and Meneveau 1999). The above expression allows for a
 314 dynamically computed value of the Smagorinsky coefficient that is consistent with
 315 local-flow properties. This local form of the dynamic Smagorinsky coefficient is nu-
 316 merically unstable ($\pm C_S^2$) due to high time correlations of $C_{S\psi}^2$ coupled with the fact
 317 that the instantaneous energy cascade can be forward or backward (Germano et al.
 318 1991). Another reason for the numerical instability is related to the assumption that
 319 $C_{S\psi}^2$ is constant over the filter width Δ . In the absence of this assumption, the model
 320 error becomes a set of integral equations. Ghosal et al. (1995) overcame this by min-
 321 imizing the integral version of the error to find $C_{S\psi}^2$ everywhere using a variational
 322 method, which was both computationally expensive and complex. The more common
 323 approach is to enforce the Germano identity in an average sense. Typically, this aver-
 324 age is enforced over some region of spatial homogeneity (e.g., over horizontal planes
 325 in a homogeneous boundary layer) which removes the $C_{S\psi}^2$ oscillations and helps to
 326 ensure numerical stability. This spatial averaging presents an issue in heterogeneous
 327 flows since the assumptions underlying the averaging procedure are violated. One
 328 approach to deal with this issue is the Lagrangian dynamic model (Meneveau et al.
 329 1996). The underlying idea of this model is that the Germano identity should be en-
 330 forced along fluid particle trajectories. A Lagrangian timescale controls how far back
 331 in time to average using 1st-order time and space estimates.

332 A second problematic assumption is that $C_{S\psi}^2$ is scale invariant (i.e., the same model
 333 and model coefficients can be used for $\tau_{ij\psi}$ and T_{ij}). While this assumption is generally
 334 reasonable provided that both filter scales Δ and 2Δ are within the inertial subrange of
 335 turbulence, it will likely be violated in some region of the flow for cases with at least
 336 one direction of flow anisotropy (e.g., the ABL). Porté-Agel et al. (2000) addressed
 337 this by developing a generalized dynamic model where $C_{S\psi}^2$ is a function of scale and
 338 made the weaker assumption that $C_{S\psi}^2$ follows a power-law distribution at the small-
 339 est resolved scales, e.g., $C_S^2(\Delta)/C_{S\psi}^2(\Delta) = C_S^2(2\Delta)/C_{S\psi}^2(2\Delta)$. Porté-Agel (2004)

340 extended this procedure to introduce the first scalar scale-dependent model and Bou-
 341 Zeid et al. (2005) combined the work of Meneveau et al. (1996) and Porté-Agel et al.
 342 (2000) and developed a scale-dependent Lagrangian dynamic model for momentum
 343 transport. Results showed that near the lower boundary the dynamic coefficient is very
 344 sensitive to the local surface roughness and that this new model better matched with
 345 experimental data than the planar-averaged formulation. Stoll and Porté-Agel (2006a)
 346 applied scale-dependent Lagrangian dynamic SGS models for both momentum and
 347 scalars to neutrally stratified boundary layers over heterogeneous terrain. These mod-
 348 els were able to accurately reproduce flow statistics and the spatial distributions of
 349 the Smagorinsky coefficients and the SGS Schmidt number in a self-consistent man-
 350 ner. In both studies and later in a detailed wind tunnel study (Carper and Porté-Agel
 351 2008), the need to locally determine coefficients in simulations of realistic ABLs was
 352 elucidated.

353 2.4 Land-surface flux models

354 Given the inertial conditions typical of the atmospheric surface layer (ASL), applica-
 355 tions of LES are overwhelmingly based upon wall-modeled closures predicated upon
 356 a TKE equilibrium conditions (Pope 2000; Piomelli and Balaras 2002). The Monin-
 357 Obukhov similarity theory (Monin and Obukhov 1954, MOST) has figured promi-
 358 nently in the proliferation of LES for atmospheric turbulence modeling, owing to its
 359 practical convenience and reliability (Stoll and Porté-Agel 2006b). Within this frame-
 360 work, surface fluxes of momentum and heat are defined, respectively, via:

$$361 \frac{\tau_{iz}^w(x, y, t)}{\rho\psi} = u_*^2 \left[\frac{\kappa U(\vec{x})}{m(\zeta)} \right]^2 \frac{\tilde{u}(\vec{x}, t)}{U(\vec{x})}, \text{ and} \quad (9)$$

$$362 \frac{Q_0}{\rho C_p \psi} = u_* \theta_* = \left[\frac{\kappa \delta\theta(\vec{x})}{h(\zeta)} \right] u_*, \quad (10)$$

363 where u_* is friction velocity, κ is the von Kármán constant, $U(\vec{x}) = (\langle \tilde{u}(\vec{x}, t) \rangle^2 + \langle \tilde{v}(\vec{x}, t) \rangle^2)^{1/2}$
 364 is the resolved velocity magnitude at the lowest computational level determined over
 365 horizontal planes, locally at each grid point, or as the local filtered value (Bou-Zeid
 366 et al. 2005; Stoll and Porté-Agel 2006b), $m(\zeta)$ and $h(\zeta)$ are the stability corrections,
 367 derived from vertical integration of the modeled non-dimensional gradients (Brut-
 368 saert 1982), where $\zeta = zL^{-1}$ is the stability parameter and $L = u_*^2 \theta_0 (\kappa g \theta_*)^{-1}$ is the
 369 Obukhov length determined in the same manner as $U(\vec{x})$, C_p is specific heat, θ_* is the
 370 so-called friction temperature, and $\delta\theta(\vec{x})$ is the local vertical thermal gradient respon-
 371 sible for convective heat fluxes. In this form, within the stability corrections, $m(\zeta)$
 372 and $h(\zeta)$, enter pre-defined lengths, $z_{0,m}$ and $z_{0,h}$, which are commonly referred
 373 to as “aerodynamic roughness lengths” and which represent the elevation at which
 374 ensemble-mean dependent quantities attain their surface values (Garratt 1992). For
 375 further discussion, interested readers may consult the recent reference text, Wyngaard
 376 (2010).

377 The wall-modeled LES paradigm offers the redeeming attribute that dependent
 378 flow quantities enter as input argument during integration of the transport equations,

379 yielding corresponding surface fluxes (i.e., Eqs. 9 and 10). Equilibrium-contingent
 380 models have well-known limitations, foremost among them being application in a
 381 space-time local sense and limitations related to the application of MOST for values
 382 of $zz_{0,m\psi}^{-1} < \mathcal{O}(10)$ in high-resolution simulations (Basu and Lacser 2017). Equations
 383 9 and 10 have utility in modeling flow over landscapes that are horizontally homoge-
 384 neous, for examples some types of agricultural fields, gently undulating topography,
 385 ice sheets, sand flats, etc. But their prognostic abilities break down with the intro-
 386 duction of relative larger-scale obstacles, for example, buildings, topographic undu-
 387 lations, sand dunes, vegetative canopies, etc. Such conditions necessitate generalized
 388 boundary conditions.

389 For flow over vegetative canopies, models based upon an *a priori* defined leaf-area
 390 index (LAI) can be added to Eq., 2 (e.g., for F_i) as a body force:

$$391 \quad F_{i\psi} = c_D a(\vec{x}) \tilde{u}_i U(\vec{x}) \quad \text{where} \quad \text{LAI} = \int_{d^2 \vec{x}\psi} a(\vec{x}) d^2 \vec{x}\psi \quad (11)$$

392 $c_D \sim \mathcal{O}(10^0)$ is a drag coefficient, and $a(\vec{x})$ is leaf-area density, which relates to LAI
 393 via the right-hand side integral in Eq. 11 (Shaw and Schumann 1992). Flows over non-
 394 porous obstacles, such as buildings or sharply-varying terrain are commonly based
 395 on an immersed-boundary method (IBM) (Peskin 1972; Mittal and Iaccarino 2005) –
 396 typically categorized as either a direct or indirect method. In applications to boundary-
 397 layer meteorology turbulence, IBM schemes typically utilize a surface closure based
 398 on surface stress (Chester et al. 2007), or some other spatial attribute of the obstacle
 399 (Anderson and Meneveau 2010; Anderson 2012).

400 In other cases, the spatial variability of an underlying landscape is too steep to be
 401 captured within an equilibrium-like model (i.e., Eq. 9), solid, but not sufficiently steep
 402 to require an IBM closure. In such scenarios, the Cartesian computational domain can
 403 be mapped to a curvilinear domain—typically from z to η , via linear transformation.
 404 This mapping introduces new terms within the momentum transport equation solver,
 405 but precludes the need for additional body forces since topographic undulations van-
 406 ish following the mapping procedure (Gal-Chen and Sommerville 1975; Clark 1977;
 407 Bao et al. 2018). It is noted, too, that solution of the mapped equations poses ad-
 408 ditional challenges for maintaining divergence-free velocity; in the Cartesian grid,
 409 divergence-free conditions are preserved via dynamic computation of a pressure cor-
 410 rection, which is itself derived from solution of a Poisson equation. Though beyond
 411 the scope of this article, it is emphasized that solution of the mapped pressure Pois-
 412 son equations requires careful treatment (Yang and Shen 2010). The aforementioned
 413 discussion addresses boundary flux modeling for momentum, but LES modeling of
 414 non-neutral turbulence also requires special treatment of the corresponding heat and
 415 moisture boundary flux. We note, for example, 1990s work on convective boundary
 416 layer flow over undulating terrain (Walko et al. 1992; Dörnbrack and Schumann 1993)
 417 and efforts to use land surface models to represent the impact of the surface energy
 418 and mass budgets (Patton et al. 2005; Huang and Margulis 2010; Shao et al. 2013).

419 3 Applications in Boundary Layer Research

420 3.1 The convective boundary layer

421 3.1.1 CBL structure and dynamics

422 Some of the earliest LES studies of the ABL focused on the daytime CBL (Dear-
 423 dorff 1970b, 1972a, 1974a,b). In a seminal paper, Deardorff (1972a) simulated neutral
 424 and convective ABLs, considering values of the global stability parameter $-z_i L^{-1} =$
 425 $0, 1.5, 4.5, 45$, where z_i is the potential temperature inversion height. Deardorff demon-
 426 strated the validity of mixed-layer scaling, where the CBL depth is characterized by z_{iW}
 427 (rather than the Ekman layer depth $u_* f^{-1}$), the stability parameter for the mixed layer
 428 is $-z_i L^{-1}$ (rather than $u_* (fL)^{-1}$), and the appropriate scales for normalizing statis-
 429 tics throughout the convective mixed layer are the convective velocity scale $w_* =$
 430 $(gz_i Q_0 / \theta_0)^{1/3}$ and the convective temperature scale $T_* = Q_0 w_* \bar{\psi}^l$. He also demon-
 431 strated that for weakly convective conditions (e.g. $-z_i L^{-1} = 4.5$), the velocity and
 432 temperature fields are organized in coherent streaks near the ground closely aligned
 433 to the mean wind direction; however, updrafts were found to be organized into open
 434 cells for more convective ($-z_i L^{-1} = 45$) conditions. Deardorff also presented pre-
 435 liminary results of dispersion in the CBL, demonstrating that vertical dispersion of
 436 neutrally-buoyant particles increases with increasing $-z_i L^{-1}$.

437 Mason (1989) performed a suite of LES of free convection, investigating the extent
 438 to which grid resolution and details of the SGS model impact the fidelity of simula-
 439 tions. He found that the domain size and grid resolution had a significant impact, and
 440 proposed a modified EV where the subgrid length scale was a function of the SGS
 441 Richardson number; this led to improved results in his simulations. Free convection
 442 was investigated further by Schmidt and Schumann (1989), with a focus on convective
 443 organization. In addition to considering vertical profiles of second- and third-order
 444 moments and velocity and temperature spectra and cospectra, they performed a de-
 445 tailed analysis of the coherent organization of the velocity and temperature fields and
 446 found that the vertical velocity and temperature fields organize into open cellular pat-
 447 terns (where several updrafts meet at a “hub”), with a horizontal length scale of $\sim 2z_i$,
 448 and with updrafts and downdrafts extending throughout the depth of the CBL.

449 Free convection also served as the basis for one of the first ABL LES intercompar-
 450 ison studies. Nieuwstadt et al. (1993) compared four different numerical simulation
 451 codes with different discretization schemes and SFS models. They found that even at
 452 the low resolution used ($\sim 6.4 \times 10^4$ grid points), profiles of boundary layer statis-
 453 tics were consistent across the participating models demonstrating that LES could be
 454 reliably used to study ABL dynamics. The good agreement was attributed to the domi-
 455 nance of large-scale thermals that are easily resolved by LES. In a follow-up study
 456 using the same four numerical codes, Andren et al. (1994) examined the impact of
 457 shear using the case of a neutrally stratified Ekman layer. They found that with the
 458 absence of large-scale thermals the numerical codes showed significant deviations
 459 from each other and, based on sensitivity tests, that the differences were largely at-
 460 tributed to differences in SFS model formulation. Fedorovich et al. (2004) performed
 461 an intercomparison using forcing conditions that combined shear and convection in an

462 attempt to understand some of the contradictory conclusions of previous work on CBL
463 entrainment. They found relative consistency in ABL statistical profiles for first-order
464 statistics with increasing scatter between numerical codes with increasing statistical
465 order. The relatively good agreement among models compared to earlier intercompar-
466 isons could have been a result of the significant increase in resolution afforded by a
467 decade of time ($\sim 6.5 \times 10^6$ grid points) or because the inclusion of any convection
468 with or without shear results in significant energy at resolved length scales.

469 Prior to Fedorovich et al. (2004), Moeng and Sullivan (1994) investigated the
470 question of how buoyancy and shear together influence CBL structure and dynamics
471 by running a suite of LES for $-z_i L^{-1} = 0, 1.4, 1.6,$ and 18 by independently varying
472 the geostrophic wind U_g and the surface heat flux. They considered the instantaneous
473 organization of the velocity field—finding similar results to Deardorff (1972a)—and
474 additionally considered vertical profiles of second- and third-order moments, and the
475 TKE budget. They proposed that the appropriate velocity scale for moderately con-
476 vective CBLs could be formed from the convective velocity scale w_* and the friction
477 velocity, i.e. $w_{m\psi}^3 = w_*^3 + 5u_*^3$. The question of how the interplay of shear and buoy-
478 ancy together impact the large-scale organization of the CBL was considered further
479 by Khanna and Brasseur (1998), who simulated CBLs with stabilities ranging from
480 $-z_i L^{-1} = 0.44$ to 730 . Based on their analysis of LES results, they proposed a mech-
481 anism whereby the organization of warm fluid ($\theta\psi > \psi\theta$) in low-momentum streaks
482 ($u' < 0$) under weakly-convective (small $-z_i L^{-1}$) conditions leads to the development
483 of horizontal convective rolls aligned 10 – 20° to the left of the mean wind direction.

484 LES also has been used to investigate the structure of the entrainment zone in the
485 CBL (Sullivan et al. 1998; Conzemius and Fedorovich 2006; Kim et al. 2003), which
486 is challenging to observe. Sullivan et al. (1998) performed LES of shear-free CBLs
487 with grid nesting near the inversion layer, in order to investigate entrainment dynam-
488 ics. They found that convective plumes played a key role in the entrainment process.
489 For weakly stratified inversion zones (low Ri), rotational motions due to penetrating
490 convective plumes led to folding of the inversion interface; however, stronger strati-
491 fication (larger Ri) prevented this folding, and smaller-scale turbulent mixing led to
492 the entrainment of warm air. Conzemius and Fedorovich (2006) conducted a suite of
493 LES experiments to study how the dynamics of the entrainment layer and associated
494 CBL development were affected by the presence of shear. They found that entrain-
495 ment zone shear played a larger role in enhancing CBL entrainment than did surface
496 shear. The authors in *op. cit.* also showed that the sheared entrainment zone exhibited
497 a layer where shear and buoyancy effects were balanced, which regulated the CBL en-
498 trainment. Work by Kim et al. (2003) focused on entrainment in sheared CBLs (the en-
499 trainment heat flux is known to be larger under sheared convection). They found strong
500 linear vortices occur in the entrainment layer for sheared convection, with locations
501 coinciding with those of horizontal convective rolls. Furthermore, Kelvin-Helmholtz
502 (K-H) wave-like billows were found in the entrainment layer, over strong updraft re-
503 gions; the K-H billows were found to lead to the enhanced entrainment heat flux in
504 sheared convection.

505 Other LES studies of the CBL have considered diverse topics, such as the extent to
506 which baroclinicity impacts mean vertical profiles and turbulence (Sorbjan 2004) and
507 the validity of (and deviations from) MOST under convective conditions (e.g., Khanna

508 and Brasseur 1997; Li et al. 2018). These studies have indicated the potential influence
 509 of an additional dimensionless parameter related to the outer length scale (i.e. zz_{ψ}^l)
 510 and suggested that coherent updrafts and downdrafts may be responsible for deviations
 511 from MOST. LES was used by Kanda et al. (2004a) to investigate surface energy
 512 balance closure in the CBL; they found that the temporally-averaged sensible heat
 513 flux ($\langle w'\theta' \rangle$) systematically underestimated the horizontally spatially-averaged heat
 514 flux, which led to a systematic bias in the surface energy budget. Other studies have
 515 used LES to investigate and characterize the statistics associated with CBL turbulence
 516 (e.g., Gibbs and Fedorovich 2014a,b).

517 Sullivan and Patton (2011) revisited the question of the extent to which grid resolu-
 518 tion impacts CBL statistics in LES, performing simulations of the shear-free CBL
 519 at resolutions ranging from 32^3 to 1024^3 . They found that filter widths $\Delta < \psi z_i / 60$
 520 (corresponding to their 256^3 simulations) were necessary to obtain statistical conver-
 521 gence for first- and second-order moments in the interior ($0.1 \leq zz_{\psi}^l \leq 0.9$) of the
 522 domain. Furthermore, they found estimation of vertical velocity skewness required
 523 filter widths of $\Delta < \psi z_i / 113$. While Sullivan and Patton (2011) employed a subgrid
 524 model based on solution to the SGS TKE equation, grid convergence tests using other
 525 SGS models (e.g. Salesky et al. 2017) indicate that grid resolution requirements for
 526 accurate LES of the CBL are sensitive to the choice of SGS model.

527 Recently Salesky et al. (2017) used LES to investigate the transition from hori-
 528 zontal convective rolls to open cells in the CBL (and the associated implications for
 529 momentum and heat transport). LES has also been used to examine the extent to which
 530 the topology of large- and very-large-scale motions (which are well-characterized in
 531 neutrally-stratified engineering flows, Hutchins and Marusic 2007) is modified by
 532 buoyancy and how these structures modulate the amplitude of small-scale turbulent
 533 fluctuations in the CBL with increasing unstable stratification (Salesky and Anderson
 534 2018), corroborating studies based on aircraft observations (Lemone 1976).

535 3.1.2 CBL modeling and parametrization

536 In addition to being used to advance the community's understanding of CBL physics,
 537 LES has also been used extensively to develop, validate, and improve parametrizations
 538 of the CBL for numerical weather prediction models. Vertical transport in the CBL is
 539 asymmetric, due to the positive skewness of vertical velocity ($\text{Sk}(w) = \langle w'^3 \rangle \langle w'^2 \rangle^{-3/2} > \psi$
 540 0) which arises because the flow field is comprised of intense updrafts that take up a
 541 small volume fraction of the flow, and larger regions of less intense downdrafts. No-
 542 tably, heat and scalar fluxes (e.g. $\langle w'\theta' \rangle$) in the convective mixed layer occur in spite
 543 of negligible mean temperature or scalar gradients (e.g. $\partial\langle\theta\rangle/\partial z$), meaning that the
 544 typical approach of modeling the flux through an eddy diffusivity, i.e.

$$545 \quad \langle w'\theta' \rangle = -K_{\theta\psi} \frac{\partial\langle\theta\rangle}{\partial z\psi} \quad (12)$$

546 fails in the mixed layer, since the eddy diffusivity $K_{\theta\psi}$ becomes ill-defined as $\partial\langle\theta\rangle/\partial z\psi \rightarrow$
 547 0. In order to ameliorate this issue, a number of investigators have used LES to explore
 548 alternatives or extensions to K -theory in the CBL.

549 Work by several authors (Wyngaard and Brost 1984; Moeng and Wyngaard 1989;
 550 Wyngaard and Weil 1991) investigated conserved passive scalars in the CBL. Notably,
 551 Moeng and Wyngaard (1989) was the first study to compare results from second-
 552 order CBL parametrizations schemes with LES data. The authors found, among other
 553 things, that downgradient diffusion closures for turbulent transport were inadequate
 554 due to the influence of buoyancy in the CBL. In total, these studies demonstrated that
 555 conserved passive scalar statistics can be represented as a superposition of “bottom-
 556 up” processes (due to upward transport and mixing) and “top-down” processes, related
 557 to entrainment. A key finding was that the top-down scalar flux ($\langle w'\theta'\rangle_t$) has a well-
 558 behaved turbulent diffusivity, but the turbulence diffusivity of the bottom-up scalar
 559 flux ($\langle w'\theta'\rangle_b$) has a singularity in the mixed layer. Wyngaard and Weil (1991) pro-
 560 posed that nonlocal bottom-up scalar transport (i.e. due to updrafts) could be modeled
 561 in terms of the vertical velocity skewness $Sk(w)$ and the vertical gradient of the scalar
 562 flux, $\partial\langle w'\theta'\rangle/\partial z$.

563 Ebert et al. (1989) proposed to represent nonlocal transport in the CBL in terms
 564 of what they referred to as transilience theory, where nonlocal mixing can be repre-
 565 sented by a matrix of mixing (or transilience) coefficients $[c_{ij}(t, \Delta t)]$ that represent
 566 the fraction of air that travels from source level i to destination level j over some time
 567 period Δt ; LES was used to evaluate these mixing coefficients. They found signifi-
 568 cant asymmetry in vertical mixing; over several large eddy turnover times, the mixing
 569 coefficients indicated removal of nearly all surface air, with a large amount of slow
 570 downward transport. As indicated by other studies, Ebert et al. (1989) found that K -
 571 theory breaks down for vertical transport in the CBL.

572 Building upon ideas presented in Deardorff (1972b), Holtslag and Moeng (1991)
 573 proposed including a counter-gradient term in the bottom-up eddy diffusivity for heat,

$$574 \quad \langle w'\theta'\rangle = -K_{\theta\psi} \left(\frac{\partial\langle\theta\rangle}{\partial z\psi} - \theta_{\psi} \right) \quad (13)$$

575 where the counter-gradient term $\theta_{\psi} = C\langle w'\theta'\rangle_0/w_* h_{\psi}$ can be related to the surface
 576 flux $\langle w'\theta'\rangle_0$. Using LES, they demonstrated that the bottom-up scalar diffusivity is
 577 well-behaved when the counter-gradient term is included, meaning that an equation
 578 of the form of Eq. (13) could be implemented in weather forecasting models.

579 Other studies have used LES to develop CBL parametrizations based on a mass-
 580 flux type approach (e.g. Randall et al. 1992; Siebesma et al. 2007), which considers
 581 the vertical transport (of heat or scalar) due to updrafts or downdrafts. This is typi-
 582 cally accomplished by including an additional term in the eddy diffusivity formulation
 583 (Siebesma et al. 2007), i.e.

$$584 \quad \langle w'\theta'\rangle = -K_{\theta\psi} \frac{\partial\langle\theta\rangle}{\partial z\psi} + M(\theta_{\psi} - \langle\theta\rangle) \quad (14)$$

585 where M is the mass flux and θ_{ψ} is potential temperature in updraft regions. The mass
 586 flux and updraft fraction in Eq. 14 can be evaluated directly from LES output to inform
 587 the development of weather and climate model parametrizations.

588 Ayotte et al. (1996) also used LES to evaluate the fidelity of CBL closure models
 589 for use in weather and climate forecasting. They ran a suite of 10 LES of the CBL
 590 encompassing free convection, sheared convection, baroclinic CBLs, and an Ekman

591 layer simulation. Several classes of CBL closure models were evaluated, including
 592 those where the eddy viscosity was specified as a function of stability (i.e. $K(Ri)$), K -
 593 profile models, mixed-layer models, Mellor-Yamada 2.0 and 2.5 order closure models,
 594 and a transilience model. The authors noted that the closure models had significantly
 595 different treatment of the entrainment zone, leading to widely varying prediction of
 596 quantities in the mixed layer. Thus, LES of the CBL has become instrumental as a
 597 tool for both developing new parametrizations.

598 3.2 The stable boundary layer

599 The study of the stratified ABL has been an area of continuous interest since the emer-
 600 gence (~ 1990) of LES as a prominent technique for inquiries into the physics of ABL
 601 turbulence. A common thread has been a focus on the capability of LES to faith-
 602 fully represent the physics of turbulent transport in the presence of stratification. The
 603 challenge lies in the representation of the SFS stress and flux under weak turbulence
 604 conditions when typical SFS model assumptions including isotropic behavior at the
 605 filter scale are not valid.

606 The first LES of the SBL was performed by Mason and Derbyshire (1990). A basic
 607 domain and simulation forcing was used that effectively consisted of a pressure driven
 608 channel flow simulation with a negative sensible heat flux prescribed at the surface.
 609 The adopted modeling strategy was very similar to previous simulations of neutral
 610 (Mason and Callen 1986) and convective (Mason 1989) boundary layer simulations
 611 and used the Smagorinsky-Lilly closure (Eq. 6). The primary modification to the SGS
 612 model for SBL simulations was the inclusion of a Ri based stability correction. This
 613 idea had been introduced previously (e.g., Deardorff 1980) but this is one of the earli-
 614 est instances specifically for the purpose of simulating stratified turbulence. Although
 615 some aspects of the simulation setup were later shown to be undesirable (e.g., constant
 616 flux surface boundary conditions discussed in Basu et al. 2008a; Gibbs et al. 2015),
 617 basic agreement between theory (i.e., Nieuwstadt 1984) and the simulation results
 618 established that LES of the SBL was possible.

619 Since these first SBL simulations, considerable effort has focused on the develop-
 620 ment and validation of SGS models. Brown et al. (1994) tested the stochastic backscat-
 621 ter model of Mason and Thomson (1992) in SBL LES and concluded that the inclu-
 622 sion of backscatter in the SGS model improved the agreement with the local-scaling
 623 hypothesis (Nieuwstadt 1984) by preventing the local collapse of turbulence that can
 624 occur in poorly resolved regions of a SBL with standard versions of the Smagorinsky-
 625 Lilly closure. Andren (1995) and Galmarini et al. (1998) examined the fidelity of
 626 higher-order closure models that were effectively LES versions of the Mellor and Ya-
 627 mada (1974) 1.0 closure. These models closely resembled the model introduced by
 628 Sullivan et al. (1994) with SBL specific SGS flux corrections. Both found that the
 629 inclusion of prognostic equations for the SGS fluxes improved agreement with local
 630 scaling and alleviated the need for a stochastic component. Saiki et al. (2000) directly
 631 implemented the model of Sullivan et al. (1994) with the SGS length scale modified
 632 following Deardorff (1980). Although a significant number of early LES of the SBL
 633 used a length scale of the form $\ell = \min(\Delta, 1/2\sqrt{EN^{-1}})$, recent work has indicated

634 that this is likely incorrect for anything but very coarse resolution LES (Gibbs and
635 Fedorovich 2016). Saiki et al. (2000) used a similar simulation setup to past work
636 but with a significantly larger geostrophic wind speed and a larger domain. Besides
637 reporting that modifications to the original scheme improved agreement with theory,
638 Saiki et al. (2000) reported on wave interactions at the boundary layer top and the
639 impact of these interactions on the structure of flow in the boundary layer. This was
640 not the first reporting of wave-turbulence interactions (e.g., Andren 1995) but it was
641 an early example of a transition from the majority of work in the 90s focusing on the
642 ability of LES to represent the SBL to an examination of SBL physics.

643 The transition to using LES as a research tool to examine SBL physics coincided
644 with a move towards the simulation of quasi-steady SBLs with conditions inspired
645 by ABL observations. Pioneering in these efforts was the work of Kosović and Curry
646 (2000) who used data from the Beaufort Sea Arctic Stratus Experiment to motivate an
647 ensemble of LESs with a short enough inertial oscillation period to reach equilibrium
648 fast enough with the computational power available at the time. These simulations
649 can be viewed as delineating a break between ABL LES of stratified turbulence and
650 the channel flow simulations favored in the engineering literature at the time (e.g.,
651 Armenio and Sarkar 2002).

652 The most important lasting contribution of Kosović and Curry (2000) is that their
653 simulation setup became the basis for the first intercomparison of LES models for
654 the SBL as part of the Global Energy and Water Exchanges (GEWEX) ABL study
655 (GABLS1, Beare et al. 2006). The intercomparison examined the performance of 11
656 different LES models with various numerics and SGS modelling schemes. The simu-
657 lations were run for a range of resolutions (depending on participants) and compared
658 to theory, field data, and a high resolution “benchmark” case. The study found that
659 for moderate stratification ($L\delta^{-1} \approx 1.5$, where δ is the boundary layer height), LES
660 can successfully represent the quasi-steady SBL. This conclusion was based on the
661 relative convergence of results from the various LES models at a sufficient resolution
662 and the agreement of the ensemble of simulations with data and theory.

663 The GABLS1 intercomparison established a strong basis for the use of LES to
664 examine weak to moderately stable ABLs and became a benchmark for the evalu-
665 ation of single column models (Cuxart et al. 2006; Svensson and Holtslag 2009),
666 the development of LES SGS models (e.g., Stoll and Porté-Agel 2008; Matheou and
667 Chung 2014), and for the examination of the physics of turbulent fluxes (e.g., Basu
668 et al. 2006; Steeneveld et al. 2007; Huang and Bou-Zeid 2013; Sullivan et al. 2016).
669 While SGS model development continued, this also marked a transition to using LES
670 to examine the physics of turbulence and towards increasingly complex simulation
671 setups. For example, Basu et al. (2006) combined results from the GABLS1 study
672 with field data to examine the applicability of MOST and Steeneveld et al. (2007)
673 used the GABLS1 results with experimental data to evaluate diagnostic models for
674 boundary layer height. Huang and Bou-Zeid (2013) used the GABLS1 case as a basis
675 for an expanded study of the impact of stratification on the structure of the ABL. Be-
676 sides general observations of the impact of increasing stratification on boundary layer
677 depth and transport characteristics, they also examined the local-scaling hypothesis
678 and found that the concept of z-less scaling (Mahrt 1999) applied at a lower level than
679 typically assumed. The work of Sullivan et al. (2016) used very high resolution simu-

680 lations of the GALBS1 case for a detailed examination of the structure of turbulence
 681 in the SBL. They identified three-dimensional inclined vortical structures similar to
 682 those identified in the neutral ABL (e.g., Carper and Porté-Agel 2004) and linked
 683 these to temperature ramps observed in the simulations and in field studies.

684 Researchers also began to add a wider range of atmospheric forcing conditions to
 685 their simulations to explore the implications on boundary layer dynamics and mod-
 686 eling. Mirocha and Kosović (2010) used LES to analyze the impact of subsidence
 687 on mixing in the SBL. The simulations were motivated by field observations and
 688 demonstrated that even very weak subsidence can have a strong impact by limiting
 689 the growth of the boundary layer height and significantly reducing mixing and cooling
 690 in the boundary layer. Additionally, they found that the inclusion of subsidence im-
 691 proved the agreement between simulations and observations. Richardson et al. (2013)
 692 created a SBL LES database that included a wide range of atmospheric forcing condi-
 693 tions to examine boundary layer height formulations. Most recently, LES SBL work
 694 has transitioned towards the very stable ABL with simulation of long-lived boundary
 695 layers in Antarctica at Dome C Station (van der Linden et al. 2019). These simula-
 696 tions demonstrated that LES can move into the space of very stable boundary layers
 697 but only at the expense of very high resolution.

698 3.3 Transitional ABLs

699 In addition to studies of the structure and dynamics of the CBL and SBL under quasi-
 700 steady forcing, LES has also been used to understand the details of the morning tran-
 701 sition, evening transition, and full diurnal cycle of the ABL.

702 Sorbjan (2007) considered growth of the CBL through the morning transition, by
 703 simulating an initially shallow CBL and forcing simulations with an increasing sur-
 704 face heat flux. He demonstrated that the mean wind shear and temperature gradients
 705 remained constant throughout the lower half of the mixed layer, but evolved in time
 706 in the upper half of the mixed layer and interfacial layer due to entrainment. Beare
 707 (2008) investigated the full morning transition from a SBL to a CBL by spinning up
 708 SBL simulations on a smaller domain, then using this as the initial condition for the
 709 morning transition. The morning transition was found to be highly sensitive to shear
 710 in its early stages, and a so-called “mixed CBL-SBL” was observed, where a shallow
 711 CBL was capped by a shear-driven SBL. Beare found that the depth of the overlying
 712 SBL increased with increasing geostrophic wind, indicating that the SBL cannot be
 713 neglected in understanding or modeling the morning transition.

714 Nieuwstadt and Brost (1986) considered the decay of turbulence in the CBL by
 715 running LES to reach steady state, then abruptly setting the surface heat flux to zero.
 716 They found that the temperature variance $\langle \theta'^2 \rangle$ decayed first (from the bottom up),
 717 followed by the vertical heat flux $\langle w'\theta' \rangle$ (also from the bottom up), the vertical veloc-
 718 ity variance $\langle w'^2 \rangle$, and finally the horizontal velocity variances $\langle u'^2 \rangle$ and $\langle v'^2 \rangle$. The
 719 ratio of time to the large eddy turnover time $t/T_{LE} = tw_*/z_{i\psi}$ was found to be the ap-
 720 propriate timescale to characterize the decay process. Sorbjan (1997) considered the
 721 more realistic case of a gradually decreasing surface heat flux, demonstrating that the
 722 decay rate of TKE depended on the both the rate of decrease of the surface heat flux

723 and the large eddy turnover timescale w_*/z_i . Pino et al. (2006) also considered the
724 evening transition (focusing on sheared CBLs), finding that wind shear increased en-
725 trainment during the transition, and that the horizontal velocity variances decay much
726 more slowly than the vertical velocity variance, leading to an increase of anisotropy
727 during the transition.

728 The first LES of the full diurnal cycle was performed by Kumar et al. (2006), using
729 idealized timeseries of surface heat flux $w\theta_0$ and geostrophic wind U_{yg} derived from
730 surface observations as forcings. They found that simulation results produced good
731 agreement with expected behavior of entrainment, CBL growth, and development of
732 a nocturnal jet. They also found that velocity variances, TKE, and the dynamically cal-
733 culated Smagorinsky coefficient $C_{S\psi}$ exhibited hysteresis-like behavior when normal-
734 ized by ΔL^{-1} ; however, this hysteresis was negligible when statistics were normal-
735 ized by $\Delta\Lambda^{-1}$, where Λ is the local Obukhov length (Nieuwstadt 1984), strongly support-
736 ing Nieuwstadt's local scaling hypothesis. Basu et al. (2008b) used a locally-averaged
737 version of the dynamic model for both momentum and heat SGS fluxes (Kumar et al.
738 2006, only used the model for momentum) and found that it was able to accurately
739 capture behavior of the diurnal transition of the ABL. Later work by Kumar et al.
740 (2010) investigated the impact of surface boundary conditions and geostrophic forc-
741 ing on the simulated diurnal evolution of the ABL, finding that some combinations
742 of forcings worked better for recovering CBL statistics, and others worked better for
743 capturing the nocturnal SBL. They found that imposing a surface temperature (rather
744 than a surface heat flux) better captured the fluxes and nighttime profiles (in agreement
745 with Basu et al. 2008a), but concluded that coupling with a surface energy balance
746 model would be necessary to generally improve agreement between simulations and
747 observations.

748 3.4 Plant canopy flows

749 Not long after LES became a widespread technique for the study of the ABL, re-
750 searchers started to simulate the dynamics of plant canopy flows (Shaw and Schumann
751 1992). Although these first simulations used a relatively small domain, combined with
752 simulations of Kanda and Hino (1994) and Su et al. (1998), this early work on LES
753 of canopy flows established the ability of LES to reproduce some of the most salient
754 features of canopy induced turbulence and the basic models and simulation forcing
755 parameters required.

756 The basic methodology used to represent the canopy has remained largely consis-
757 tent with Eq. 11 but researchers have proposed different ways to represent both canopy
758 drag and the impact of unresolved interactions of the flow with the plant canopy. Those
759 using a form of Eq. 7 (e.g., Shaw and Schumann 1992; Kanda and Hino 1994; Dwyer
760 et al. 1997) introduced an energy sink term into the equation to represent the impact
761 energy dissipation due to unresolved plant matter. The addition of the term is consis-
762 tent with the general idea of a spectral "short circuit" of energy (Finnigan 2000; Shaw
763 and Patton 2003) from large to small scales with the form of the term closely follow-
764 ing higher-order RANS closures for plant canopies (Wilson 1988). Shaw and Patton
765 (2003) found that the form of this term is not critical within a plant canopy as a result

766 of SFS wake energy's small value compared to resolved TKE and SFS kinetic energy.
767 Other researchers have also developed methods to include unresolved or poorly re-
768 solved impacts of individual canopy components. Yue et al. (2007) developed a drag
769 model that included a classical cylinder drag component to account for subgrid (but
770 still significant) drag from the trunk of a plant and Shaw and Patton (2003) included
771 the effect of viscous (boundary layer) drag on leaf surfaces. Shaw and Patton (2003)
772 found the viscous drag component to be unimportant compared to form drag and the
773 model of Yue et al. (2007) never found favor with modelers. A more sophisticated
774 approach was developed for fractal trees by Chester et al. (2007) using an IBM to
775 represent the resolved portion of a tree and then assuming the tree is fractal, the SGS
776 drag was estimated. This method has the novel feature that it includes the impact of
777 sheltering at unresolved scales but it has not caught on outside the research group it
778 was developed in likely because drag from real trees is mostly considered to be a re-
779 sult of the LAD and in general, the distribution of leaf sizes is not fractal. An IBM
780 approach was also employed by Yan et al. (2017) and compared to wind tunnel data
781 from a model deciduous canopy. They found that a combination of an IBM model
782 for the trunk and a porous canopy drag model (e.g., Eq. 11) provide the best repre-
783 sentation. Besides work looking to capture drag due to unresolved plant components,
784 significant effort has examined the impact of plant motion on momentum transport
785 (e.g., Dupont et al. 2010).

786 The development and maturation of plant canopy LES coincided with advance-
787 ments in the experimental and theoretical understanding of canopy flows. Two topics
788 stand out from the experimental and theoretical work, the origin and role of scalar mi-
789 crofronts over plant canopies and the "mixing-layer" analogy. Scalar microfronts are
790 clearly identifiable ramp structures found most commonly in temperature timeseries
791 just above a plant canopy (e.g., Gao et al. 1989) and the "mixing-layer" analogy hy-
792 pothesizes on the dominant transport mechanism between a plant canopy and the ASL
793 by comparisons with classical mixing-layer theory (Raupach et al. 1996). LES has
794 played a critical role in elucidating these two ideas and how they are linked through
795 turbulent flow structures. This started with the work of Kanda and Hino (1994) who
796 examined the evolution of instantaneous canopy top structures and their link to TKE
797 and vertical momentum fluxes. They identified two primary canopy top structures
798 (spanwise vortical "rolls" and streamwise vortical "ribs") and associated vertical pro-
799 files of Reynolds stress and turbulence intensity with inclined structures above the
800 canopy. Fitzmaurice et al. (2004) extended this by releasing a passive scalar and ex-
801 amining the correlation of scalar ramps with pressure perturbations. They found that
802 scalar ramp structures coincided with positive peaks in the pressure and used condi-
803 tional sampling to associate the ramp structures and pressure peaks with an upstream
804 sweep zone and a downstream ejection zone. The association between pressure and
805 scalar ramps is consistent with field data and using LES; Fitzmaurice et al. (2004)
806 was able to add an understanding of the 3D velocity field associated with these ramps.
807 Instead of conditionally sampling based on pressure, Watanabe (2004) used wavelet
808 transforms to directly identify the scalar ramps. Watanabe (2004) confirmed prior
809 results and also identified a link between canopy top structures and streaks of low-
810 speed momentum similar to those identified in boundary layer flows (e.g., Hutchins
811 and Marusic 2007). Future researchers would build on these ideas and continue to use

812 LES to examine the link among scalar ramps, the mixing-layer analogy, and 3D co-
813 herent velocity structures. Finnigan et al. (2009) used the conditional averaging tech-
814 nique of Fitzmaurice et al. (2004) in a more extensive study of coherent structures
815 and their evolution over a plant canopy. They extended past work by analyzing λ_2
816 the second eigenvalue of the perturbation velocity gradient tensor (i.e., the velocity
817 gradient tensor with the mean gradient removed), and the evolution of the condition-
818 ally sampled structures. They identified a highly 3D structure associated with head-up
819 ejection generating and head-down sweep generating hairpin vortices and surmised
820 that these structures result from a helical pairing associated with the instability cre-
821 ated by the canopy top velocity inflection and that this process is largely independent
822 of the overlying turbulence in the ASL.

823 In a follow up, Bailey and Stoll (2016) used a similar simulation configuration
824 to Finnigan et al. (2009) but with structure identification from the full velocity gradi-
825 ent tensor (e.g., λ_2 following Jeong and Hussain 1995). Based on conditional averages
826 triggered on pressure perturbations, they developed an alternative theory on the evolu-
827 tion and form of canopy top coherent structures. They found a quasi 2D structure with
828 3D structures similar to Finnigan et al. (2009) superimposed on it. This was primarily
829 a consequence of identifying structures based on λ_2 instead of λ_2 (see Bailey and Stoll
830 2016, appendix for a discussion of the difference in canopy structures identified with
831 each). Additionally, they proposed a translative instability not helical pairing as the
832 primary driver of canopy flow structures and that this instability aligns with hairpin
833 “packets” (Adrian et al. 2000) and large-scale boundary layer streaks (Hutchins and
834 Marusic 2007) in the ASL above the canopy.

835 Similar to other application areas, once LES was established as a viable method
836 to examine plant canopy flows researchers quickly moved on to more realistic forcing,
837 domains, and canopy characteristics and interactions. Central to this was the inclusion
838 of horizontal canopy heterogeneity. Although not technically a plant canopy, the work
839 of Patton et al. (1998) on windbreak flows was one of the first to include horizontally
840 heterogeneous porous elements modeled using equation 11. Researchers also focused
841 on the impact of forest clearings and edges on canopy flow. For example, Cassiani
842 et al. (2008) examined both clearing-to-forest and forest-to-clearing transitions with
843 different LAI values and identified re-circulation zones at each transition. Dupont and
844 Brunet (2008) validated their simulations of a clearing to forest transition and showed
845 how increases in canopy density (LAI) shorten the adjustment zone over which tur-
846 bulence develops compared to lower density cases.

847 After these somewhat idealized cases, researchers moved to more complex canopy
848 architectures with ever increasing realism. Bohrer et al. (2009) was one of the first to
849 look at a realistic horizontal distribution of leaf area density by combining coarse air-
850 borne LiDAR with a canopy reconstruction model. They found that heterogeneity had
851 a strong impact in the vicinity of the canopy with a marked increase in flux spatial
852 correlations. Although idealized, Bailey and Stoll (2013); Bailey et al. (2014) sim-
853 ulated row-oriented crops (e.g., a grape vineyard) with resolved rows and examined
854 the impact of this heterogeneity in the limit of a sparse canopy. Comparisons be-
855 tween row-resolved and the equivalent homogeneous canopy (i.e., equal LAI) found
856 that horizontal heterogeneity has minimal impact on first-order statistics but a signifi-
857 cant impact on higher-order ones and canopy flow structures. In particular it increases

second- and third-order statistics, decreases the coherence of the flow, and both preferentially locates flow structures and for lower effective LAI, allows structures to penetrate deeper into the canopy. Boudreault et al. (2017) found similar impacts to Bailey and Stoll (2013) when using LiDAR data to examine forest-edge flow. The inclusion of realistic heterogeneity increased structure penetration at the edge and enhanced second- and third-order velocity statistics.

The inclusion of improved canopy architecture was also accompanied by efforts to improve and study the impact of more realistic forcing conditions and coupled canopy-atmosphere exchanges. General diurnal effects of plant canopies (Aumond et al. 2013) and detailed assessment of the impact of convection on turbulence statistics, coherent structures, and canopy atmosphere interactions (Huang et al. 2009; Patton et al. 2016) where all studied. More recently, the impact of canopy heterogeneity and diurnal forcing conditions have been combined in simulations of a realistic semi-arid forest (Kröniger et al. 2018).

3.5 Dispersion and urban flows

Due to its importance for air quality and human health (Fenger 1999; Zhang et al. 2015), and impact on both the ABL and large-scale weather systems (Hildebrand and Ackerman 1984; Shepherd 2005; Niyogi et al. 2011), urban meteorology has long been a topic of interest for the ABL research community; LES investigations of the urban boundary layer (UBL) started in the early 2000s. Notably, LES was first applied to urban meteorology several decades later than canonical ABL flows, due to the additional complexity required to resolve the impacts of individual buildings on momentum and scalar transport. The earliest urban LES studies used finite volume or finite element methods with boundary-fitted grids (Hanna et al. 2002; Walton and Cheng 2002). IBMs have become popular recently (Tseng et al. 2006; Bou-Zeid et al. 2009; Giometto et al. 2017) due to their relatively low computational expense, and the fact that one can retain an underlying discretization on a Cartesian grid.

3.5.1 Urban meteorology

In contrast to the ABL over flat, horizontally homogeneous terrain, the urban canopy layer (UCL) features additional complexities, including: 1) reduced mean wind speeds within the UCL due to drag forces on buildings, 2) a region of elevated shear at the top of the UCL, 3) production of small-scale turbulence in the wake of buildings, 4) significant spatial heterogeneity in the flow, which leads to additional terms (i.e. dispersive stresses and fluxes) in the governing equations, 5) a complex surface energy budget with heterogeneous heating and cooling of the ground and building walls, and 6) heterogeneous sources and sinks of scalars (water vapor, greenhouse gases, aerosols, etc.). These complexities make the collection and interpretation of field data extremely challenging (Pardyjak and Stoll 2017). In contrast, LES is free from many of the limitations of measurement systems and ideally suited for UBL studies.

The majority of urban LES studies have focused on urban street canyons (e.g. Walton and Cheng 2002; Cui et al. 2004) or arrays of cuboids (e.g. Kanda et al. 2004b;

899 Kanda 2006; Philips et al. 2013) (typical of European and North American cities,
 900 respectively); a particular topic of interest in many urban LES studies is the extent
 901 to which geometric properties, such as the aspect ratio of street canyons or height
 902 distribution, alignment, and packing density of cuboids, influence the mean flow, tur-
 903 bulence, and scalar dispersion (e.g. Li et al. 2008; Cai et al. 2008; Hayati et al. 2019).
 904 Other studies have employed more realistic urban geometries (e.g. Tseng et al. 2006;
 905 Xie and Castro 2009; Bou-Zeid et al. 2009; Xie 2011; Kanda et al. 2013; Giometto
 906 et al. 2016) and recently, high-resolution LES with a significant degree of realism
 907 (Giometto et al. 2017) has become possible using techniques like airborne LiDAR
 908 that can measure urban geometry including trees and buildings at sub-meter resolu-
 909 tion.

910 Early LES work on UBLs focused on characterizing the mean wind profile and
 911 turbulence statistics (velocity variances, turbulence kinetic energy, and momentum
 912 fluxes) in idealized urban geometries (e.g. Hanna et al. 2002; Kanda et al. 2004b).
 913 These simulations demonstrated that the mean velocity profile is greatly attenuated
 914 within the UCL, and the magnitude of the streamwise momentum flux $\langle u'w'\psi \rangle$ peaks
 915 near the canopy top. Kanda et al. (2004b) demonstrated that the streamwise and ver-
 916 tical velocity variances (σ_u/u_* and σ_w/u_* , respectively) change significantly with
 917 height inside the canopy; the maximum values of σ_u/u_* and σ_w/u_* within the canopy
 918 were found to increase with increasing plan area fraction $\lambda_{p\psi} = A_p/A_{T\psi}$ (where $A_{p\psi}$ is
 919 the planar area of buildings and $A_{T\psi}$ is the total area). Subsequent work used LES to
 920 characterize coherent structures in urban canopies (Cui et al. 2004; Kanda et al. 2004b;
 921 Kanda 2006). Kanda et al. (2004b) showed that the streamwise wavelength of coher-
 922 ent structures at the urban canopy top was $\lambda_x/H\psi \approx 5$ for sparsely-spaced cuboids
 923 (larger than what is found in vegetation canopies), and increases with increasing plan
 924 area fraction $\lambda_{p\psi}$. These large streamwise wavelengths indicate that the mixing layer
 925 analogy (Raupach et al. 1996) should not be expected to hold in urban canopies to the
 926 extent that it does in vegetation canopies. Using LES, Kanda (2006) demonstrated that
 927 the ratio of sweep ($u' > 0, w'\psi < 0$) to ejection ($u' < 0, w'\psi > 0$) events (i.e. S_2/S_4) in
 928 urban canopies was a factor of two larger than what has been measured in vegetation
 929 canopies.

930 In urban canopies and vegetation canopies, variables can be decomposed into a
 931 temporal mean and fluctuation, e.g. $u_{i\psi} = \overline{u_{i\psi}} + u'_{i\psi}$ and a spatial mean and fluctuation,
 932 e.g. $u_{i\psi} = \langle u_i \rangle + u''_{i\psi}$ (Finnigan 2000), due to spatial heterogeneities in the flow. One
 933 can derive the mean momentum balance equation by double averaging (in time and
 934 space), yielding

$$935 \quad \frac{\partial \langle \overline{u_i} \rangle}{\partial t\psi} + \langle \overline{u_j} \rangle \frac{\partial \langle \overline{u_i} \rangle}{\partial x_{j\psi}} = - \frac{1}{\rho\psi} \frac{\partial \langle \overline{p} \rangle}{\partial x_{i\psi}} - \frac{\partial \langle \overline{u'_i u'_j} \rangle}{\partial x_{j\psi}} - \frac{\partial \langle \overline{u''_i u''_j} \rangle}{\partial x_{j\psi}} + f_{F_{i\psi}} + f_{V_{i\psi}} \quad (15)$$

936 where $f_{F_{i\psi}}$ and $f_{V_{i\psi}}$ correspond to form drag and viscous drag, respectively. Here terms
 937 emerge containing both the Reynolds stress, $\langle \overline{u'_i u'_j} \rangle$ (due to fluctuations from the tem-
 938 poral mean) and the so-called dispersive stress, $\langle \overline{u''_i u''_j} \rangle$ (due to fluctuations from the
 939 spatial mean). Although the importance of dispersive stresses (and the corresponding
 940 scalar fluxes, e.g. $\langle \overline{u''_i \theta \psi} \rangle$) has long been surmised in urban canopies, they can only be

941 calculated from spatially-resolved measurements. LES studies (Kanda et al. 2004b;
 942 Xie and Castro 2006; Boppana et al. 2010) of flow and dispersion in urban geome-
 943 try have demonstrated that the dispersive momentum ($\langle u'w' \rangle$) and scalar ($\langle \theta'w' \rangle$)
 944 fluxes can be significant within the UCL, accounting for 30% or more of the total flux
 945 within the canopy. In simulations of flow over Basel, Switzerland, Giometto et al.
 946 (2016) found that dispersive fluxes varied significantly in space; furthermore disper-
 947 sive transport in the TKE budget was found to be non-negligible within the UCL.

948 Investigators have also found LES to be a valuable tool for developing urban
 949 parametrizations for large-scale weather and climate models. The mean velocity pro-
 950 file for a neutrally-stratified ABL in the ASL over a rough surface (i.e. above the
 951 roughness sublayer) is given as

$$\bar{U}(z) = \frac{u_*}{\kappa\psi} \ln \left(\frac{z - d\psi}{z_{0,m\psi}} \right), \psi \quad (16)$$

953 where d is the displacement height. An important question for urban parametrizations
 954 is how aerodynamic parameters ($z_{0,m\psi}$ and d) are related to properties of the urban mor-
 955 phology (Grimmond and Oke 1999), such as the mean building height ($\langle h \rangle$), maxi-
 956 mum building height (h_{max}), standard deviation and skewness of building height (σ_h
 957 and Sk_h), and the plan-area and frontal area fractions $\lambda_{p\psi}$ and $\lambda_{f\psi} = A_f/A_{T\psi}$ (where
 958 $A_{f\psi}$ is the frontal area of buildings projected in the mean wind direction). Kanda et al.
 959 (2013) ran an ensemble of over 100 LES of real urban areas (focusing on subsets of
 960 Tokyo) to create a database of turbulence statistics and surface drag corresponding to
 961 various surface morphologies. Using the database, they proposed parametrizations for
 962 $z_{0,m\psi}$ and d as a function of $\langle h \rangle$, h_{max} , σ_h , λ_p , and λ_f . Zhu et al. (2017) performed LES
 963 over synthetic urban geometry, demonstrating that $z_{0,m\psi}$ also has a non-trivial depen-
 964 dence on Sk_h , the skewness of the building height distribution. Other work (Sadique
 965 et al. 2017) has focused on how $z_{0,m\psi}$ is related to building aspect ratio by including a
 966 model for sheltering, i.e. a reduction of momentum in the wakes of individual build-
 967 ings, which affects the drag on surrounding buildings (Raupach 1992).

968 In vegetation or urban canopies, the mean velocity profile within the canopy is
 969 often assumed to follow an exponential profile (Macdonald 2000), i.e.,

$$U(z) = U_h \exp [a(z/h - 1)], \quad z \leq h, \psi \quad (17)$$

971 where U_h is the velocity at canopy top, h is the canopy height, and a is an extinction
 972 coefficient taken to be proportional to LAI (in vegetation canopies) or frontal area
 973 fraction $\lambda_{f\psi}$ in urban canopies. LES has been used to investigate the extent to which
 974 Eq. 17 (and the underlying assumptions) hold in urban canopies (Castro 2017). To
 975 derive Eq. 17, one must assume a constant drag coefficient $C_{d\psi}$ with height within
 976 the canopy, that the Reynolds stress can be modeled with a mixing length model
 977 (i.e. $-\langle u'w' \rangle = l_{m\psi}^2 (\partial U / \partial z)^2$) where the mixing length is constant with height, and
 978 that dispersive stresses can be neglected (Castro 2017). However, LES studies have
 979 demonstrated that both $C_{d\psi}$ and $l_{m\psi}$ have non-negligible variation with height within the
 980 urban canopy, meaning that Eq. 17 does not hold true in general in urban canopies.

981 LES has also been used to investigate the extent to which buoyancy modifies flow
 982 and transport in urban canopies with simulations where the ground (Li et al. 2010;

983 Boppana et al. 2014; Tomas et al. 2016) or walls (Cai 2012) are heated or cooled
984 in order to assess the impacts of stratification on the mean velocity profile, turbu-
985 lence statistics, residence time of pollutants released in street canyons, and strength
986 and structures of mean vortex circulations in street canyons. Recently, LES has been
987 coupled with energy balance models for urban areas in order to impose a realistic dis-
988 tribution of building surface temperatures and to investigate the diurnal evolution of
989 flow within the urban canopy (Yaghoobian et al. 2014; Nazarian et al. 2018).

990 An important question related to our ability to describe the geometry of urban
991 areas is the sensitivity of simulated urban flows to the details of urban geometry.
992 Bou-Zeid et al. (2009) ran simulations of a university campus, varying the repre-
993 sentation of the buildings (i.e., by combining multiple buildings for some simula-
994 tions). They concluded that a high level of building detail did not have a signifi-
995 cant impact on mean flow and aerodynamic properties—suggesting that rather coarse
996 parametrizations of building geometry are acceptable when using LES to develop ur-
997 ban canopy parametrizations for large-scale weather forecasting models. However,
998 turbulence properties were found to vary significantly with the level of building detail
999 included in simulations, indicating that high-fidelity representations of urban geome-
1000 try are necessary for understanding turbulence and dispersion.

1001 3.5.2 Urban dispersion and scalar transport

1002 In addition to studying mean flow and turbulence properties, LES has also been em-
1003 ployed to investigate urban air quality and dispersion. A significant number of these
1004 studies (Walton and Cheng 2002; Baker et al. 2004; Cai et al. 2008; Li et al. 2008,
1005 2010; Michioka et al. 2014) consider the question of how a passive scalar (or pol-
1006 lutant) released in an urban street canyon is transported vertically and the following
1007 picture has emerged. When the wind direction is perpendicular to the street canyon
1008 axis, a recirculation vortex forms in the street canyon, with its axis parallel to that of
1009 the street canyon. Secondary vortices may also form; this depends on street canyon
1010 aspect ratio $\mathcal{A} = HW^{-1}$ and thermal stratification. For neutral stratification with an
1011 aspect ratio of $\mathcal{A} \approx 1$, lower scalar concentrations are found on the downstream wall
1012 of the street canyon, where vertical profiles are nearly constant. On the upstream wall,
1013 concentration peaks near the ground, and then decreases with height zH^{-1} (Walton
1014 and Cheng 2002). For a scalar released from an area source at ground level, the verti-
1015 cal flux of scalar at canopy top ($\langle w'c\psi \rangle$) decreases with increasing canyon aspect ratio
1016 \mathcal{A} (Cai et al. 2008). For street canyons with very high aspect ratio (e.g. $\mathcal{A} > 3$), mul-
1017 tiple counter-rotating recirculation vortices form throughout the depth of the street
1018 canyon, and the vertical scalar flux at canopy top is greatly diminished compared to
1019 the $\mathcal{A} \approx 1$ case (Li et al. 2008). Ground heating facilitates pollutant removal from the
1020 street canyon. In this case, vertical buoyancy forces modify the recirculation vortex
1021 within the canyon, leading to lower scalar concentrations within the canyon and larger
1022 values of $\langle w'c\psi \rangle$ at street-canyon top (Li et al. 2010).

1023 Michioka et al. (2014) investigated the more realistic case of street canyons with
1024 finite length in the cross-stream direction, finding that as the length to height ratio
1025 LH^{-1} decreased, lateral dispersion (due to flow channeling between buildings) was
1026 enhanced, leading to decreased concentrations within the street canyon. Baker et al.

(2004) considered the case of reactive scalars, namely NO and NO₂ emitted from a line source within a street canyon (modeling emissions from traffic), with background values of ozone (O₃). They found significant spatial variability in ozone within the street canyon, which has major implications for pedestrian exposure to pollutants.

LES studies have also examined point-source scalar dispersion in idealized (cuboid arrays) or realistic urban canopies. Using an IBM, Tseng et al. (2006) simulated point-source scalar dispersion in downtown Baltimore, MD, presenting evidence of channeling of the scalar plume around buildings, and significant spatial and temporal variability of scalar concentration. Xie and Castro (2009) performed scalar dispersion simulations for central London (for the DAPPLE experiment location), finding reasonable agreement between LES and observations and significant flow channeling around buildings. In a follow-up study, Xie (2011) forced LES dispersion simulations for the DAPPLE site with realistic wind data, finding that this improved agreement between LES and observations; predicted scalar concentrations from LES were found to have a significant dependence on wind angle.

Philips et al. (2013) performed LES of point-source passive scalar dispersion over arrays of cuboids in order to investigate how urban geometry impacts scalar plume statistics. They found that staggered buildings increased lateral dispersion, whereas aligned buildings enhanced vertical dispersion. Plumes became narrower with increasing source height within the urban canopy. In addition, they found that the vertical plume spread σ_y had similar behavior for all plumes several building heights downstream, but the lateral plume spread σ_x varied significantly depending on the source location and urban geometry ($\lambda_{\psi}, \lambda_f$, and whether buildings were staggered or aligned). In other recent work, Santos et al. (2019) used LES to investigate the ratio of peak to mean concentration in urban dispersion simulations; LES output was used to estimate the value of a power-law exponent in a model relating maximum to mean concentration. However, they found that results were somewhat sensitive to the choice of SGS model and grid spacing.

3.6 Large-scale spatial heterogeneity

Landscape heterogeneities are intrinsically linked to locally-elevated surface fluxes of momentum, heat, humidity, and other quantities including pollen and dust. Such surface fluxes are a product of land-atmosphere interactions affecting the hydrologic cycle, and local heterogeneities create microclimates that profoundly alter the existence of surface layer-like conditions. Herein, we adopt the contemporary structural paradigm of ASL turbulence, wherein a hierarchy of attached eddies (as per MOST) are structurally autonomous but dynamically modulated by the passage of yet-larger structures meandering within the flow (Lemone 1976; Hutchins and Marusic 2007; Salesky and Anderson 2018). The limiting extent for attached eddies, $\lambda_{a,1} \sim \delta$, while the limiting extent for the larger-scale structures is $\lambda_{a,2} \sim 10^1 \delta \sim 10^1 \lambda_{a,1}$. In this context, spatial landscape heterogeneities can themselves be decomposed based on the characteristic length of the heterogeneities, λ_l . For $\lambda_l \delta^{-1} < \psi$ and $\lambda_l \delta^{-1} > \psi$, the landscape heterogeneity is small- and large-scale, respectively. In the case of the former, individual roughness sublayer processes are homogenized within the flow; for

1070 the latter, flow heterogeneities are persistent over the depth of the flow. The remainder
1071 of this discussion is devoted to the latter.

1072 Landscape heterogeneities occur via spatial variation in aerodynamic, thermal,
1073 and moisture conditions. For simplicity, these different landscape conditions are dis-
1074 cussed separately starting with the use of LES to determine large-scale response to
1075 canonical variation in aerodynamic conditions. For the scenario in which the pre-
1076 vailing wind direction is aligned to encounter a streamwise step-change in surface
1077 roughness, from z_{0-} to z_{0+} (where z_{0-} to z_{0+} are surface roughness lengths), a sig-
1078 nificant body of knowledge exists on the resulting flow field. If $z_{0+} > z_{0-}$ (the smooth-
1079 to-rough transition), an internal (momentum) boundary layer (IBL), δ_i , forms at the
1080 transition and grows in thickness downwind of the transition (Brutsaert 1982). Di-
1081 mensional analysis (Garratt 1990) has indicated that δ_i is dependent on downwind
1082 position, x , and z_{0+} as first expressed by the Wood (1981) model:

$$1083 \quad \delta_i(x, z_{0+}) = C z_{0+} \left(\frac{x\psi}{z_{0+}} \right)^n, \psi \quad (18)$$

1084 where field and experimental data generally have indicated $C\psi = 0.28$ and $n\psi \approx 0.8$
1085 (Antonia and Luxton 1971). Further, the abrupt transition in roughness results in an
1086 abrupt rise in surface stress, and elevated production of turbulence in the fluid immedi-
1087 ately above and downwind of the transition (Antonia and Luxton 1971; Bou-Zeid et al.
1088 2004). These effects introduce mean flow disturbances, which change the boundary
1089 layer and prevent reduction of the momentum transport equations under the horizontal
1090 statistical homogeneity assumption, $\partial\langle\tilde{u}_i\rangle_{xy}/\partial x\psi \neq \partial\langle\tilde{u}_i\rangle_{xy}/\partial y\psi \neq \langle\tilde{v}\rangle_{xy\psi} = \langle\tilde{w}\rangle_{xy\psi} = 0$
1091 for $i = 1-3$ (Belcher et al. 2012). Bou-Zeid et al. (2004) ran a comprehensive LES para-
1092 metric study to evaluate the effects of changing the aerodynamic roughness lengths,
1093 and the width of high-roughness streamwise heterogeneous “strips”, while Bou-Zeid
1094 et al. (2007) considered yet more complex scenarios of topographies composed of
1095 squares of varying roughness. These studies found that the average momentum fluxes
1096 are well characterized by an effective aerodynamic roughness $z_{o,e}$.

1097 The influence of spanwise-varying surface stress has gained substantial interest in
1098 recent years, although prior efforts have been directed towards hydraulic engineering
1099 applications (open channel flows) or to fundamental wall turbulence studies. Studies
1100 have shown that there is a high degree of spanwise heterogeneity in the mean flow
1101 when the surface roughness features a prominent spanwise heterogeneity (Nugroho
1102 et al. 2013; Willingham et al. 2013; Anderson et al. 2015; Yang and Anderson 2017;
1103 Hwang and Lee 2018; Anderson 2019b). This research has revealed that elevated
1104 drag across “rough” regions induces spatial heterogeneities in the Reynolds (turbu-
1105 lent) stresses (Tennekes and Lumley 1972; Pope 2000). It has been shown (Anders-
1106 son et al. 2015) that a turbulence production-dissipation imbalance above the “rough”
1107 zones necessitates a downwelling of momentum from aloft (Hinze 1967), which thus
1108 necessitates a lateral outflow and corresponding upwelling across the “smooth” ar-
1109 eas. More recently, intermediate cases wherein the landscape heterogeneity is aligned
1110 oblique to the main transport direction have been considered (Anderson 2019a).

1111 Research examining ABL response to thermal and moisture heterogeneities at the
1112 land surface has largely focused on the CBL using either idealized or data driven pat-
1113 terns of surface sensible heat flux, potential temperature, surface moisture, or some

1114 combination. Early studies used one- or two- dimensional sinusoidal patterns to ex-
1115 amine how heterogeneity wavelength (λ_l) and amplitude impacted CBL fluxes (Had-
1116 field et al. 1992; Shen and Leclerc 1995; Avissar and Schmidt 1998; Baidya Roy and
1117 Avissar 2000). These studies established that only wavelengths $\lambda_l > \delta$ had an appre-
1118 ciable impact on horizontally averaged vertical fluxes and boundary layer turbulence
1119 statistics. For all values of λ_l , stronger background winds decreased the impact of het-
1120 erogeneity and all studies observed turbulence enhancements over the flux maxima,
1121 including enhanced updrafts and enhanced values of the velocity and potential tem-
1122 perature variances near the surface. Which velocity components were impacted the
1123 most depended on if the heterogeneity pattern was one or two dimensional (Shen and
1124 Leclerc 1995; Courault et al. 2007). The primary explanation for observed flux and
1125 variance enhancements was secondary circulations resulting from localized pressure
1126 gradients created by horizontal temperature differences. With stronger background
1127 winds, these pressure gradients wash out. As the strength of the organized circula-
1128 tions increases, they were found to countervail the random patterns observed in ho-
1129 mogeneous CBLs (Avissar and Schmidt 1998, see Sect. 3.1.1 for homogeneous CBL
1130 dynamics). Importantly, the signature of homogeneous CBL turbulence is not elimi-
1131 nated by this process, it is simply hidden in time averaged fields (Baidya Roy and Avis-
1132 sar 2000). What constitutes a strong background wind depends on the orientation of
1133 the winds with respect to the heterogeneity patterns. Raasch and Harbusch (2001) re-
1134 ported measurable impacts, even under strong background winds, with checkerboard
1135 heterogeneity when the winds aligned with the diagonals of the surface flux pattern.
1136 Furthermore, Courault et al. (2007) reported that spanwise homogeneous strips had
1137 an enhanced impact compared to checkerboard type patterns and that using a model
1138 that couples the surface state variables to the ABL appears to dampen the signature
1139 of surface heterogeneity by lessening flux contrasts.

1140 Natural patterns derived from aircraft and satellite based remotely sensed surface
1141 conditions have also been explored. One of the first was Hechtel et al. (1990) who used
1142 surface sensible and latent heat flux heterogeneity distributions chosen to match the
1143 spectra of measured surface temperature distributions taken from aircraft flight tran-
1144 sects. The simulations had modest agreement with measurements and did not differ
1145 significantly from an equivalent homogeneous run. A few possible explanations for
1146 the lack of sensitivity were given: poor simulation characteristics (SGS models, grid
1147 resolution), presence of background winds, and the small value of λ_l (only slightly
1148 larger than the grid scale). Various levels of coupling between the land surface and
1149 the ABL through either a two-source model (Albertson et al. 2001; Kustas and Al-
1150 bertson 2003), or a full land surface model (Huang and Margulis 2010) have also been
1151 explored. These simulations generally agreed with field measurements supporting the
1152 idealized study conclusions that heterogeneity length scales smaller than δ have min-
1153 imal impact on CBL fluxes. Kustas and Albertson (2003) examined the impact of
1154 surface temperature contrast with their model and found that enhanced contrast did
1155 not appreciably impact horizontally averaged fluxes. They surmised that this was a
1156 result of the feedback between secondary circulations and surface fluxes allowed by
1157 coupled models in agreement with more idealized studies (Courault et al. 2007).

1158 In contrast to the neutral heterogeneous ABL discussed above, in the heteroge-
1159 neous CBL the impact of heterogeneity is found to propagate up through the ASL for

1160 sufficiently large λ_{ly} with both idealized and realistic heterogeneity patterns (Baidya Roy
1161 and Avissar 2000; Huang and Margulis 2010; Maronga and Raasch 2013). This inval-
1162 idates the concept of a “blending-height” used in mosaic, tile, and many bulk methods
1163 that researchers have found to be successful in heterogeneous neutral and stably strat-
1164 ified ABLs (e.g., Bou-Zeid et al. 2004; Miller and Stoll 2013).

1165 **4 Future of LES**

1166 **4.1 Simulation Scaling Trends**

1167 The history and usage of LES for ABL applications is tied to the development of mod-
1168 ern computing. One measure researchers have used to link computational physics to
1169 advancements in computing is to examine the scaling relationship between the max-
1170 imum number of grid points used in a simulation and the years since activities com-
1171 menced (Voller and Porté-Agel 2002; Bou-Zeid 2015). We performed this analysis for
1172 all the identifiable LES papers published in BLM (Fig. 4). Our analysis was restricted
1173 to BLM so that it would be representative of research efforts in the ABL community
1174 and the trajectory of work published in the journal. Articles that used LES data from
1175 other publications were not included to remove any biases in timing that might emerge
1176 from data reuse. Additionally, articles in which the maximum number of grid points
1177 could not be readily identified were skipped (see the Online Resources for DOIs of all
1178 articles used in Fig. 4). Although the first simulations were run in the 1970s, scaling
1179 fits to Moore’s Law were done starting from 1990 when the trend in the number of
1180 simulations per year increased. Fits prior to this produce highly variable results due
1181 to the extremely low number of samples per year.

1182 It is immediately evident from Fig. 4 that, on average, LESs published in BLM do
1183 not follow Moore’s Law. While it is questionable if Moore’s Law will hold into the
1184 future, it has been approximately valid for the range of years we studied (Khan et al.
1185 2018). Interestingly, the scaling exponent (0.27) is close to that found for DNSs from
1186 JFM (Bou-Zeid 2015). Although the best-fit trend does not follow Moore’s Law, there
1187 are simulations that do, indicating it was possible during the study period.

1188 Of interest is why the best-fit trend is well below Moore’s Law. One possible expla-
1189 nation is that LES users frequently choose to run simulations using fewer grid points
1190 out of convenience. This could be out of a desire to use available desktop computing
1191 resource instead of shared high-performance computing (HPC) systems, or to avoid
1192 the hassle associated with the analysis of the extremely large datasets that result from
1193 running biggest-possible simulations. The similar scaling exponent to that found for
1194 DNS suggests otherwise if it is assumed that researchers are not purposefully targeting
1195 lower Reynolds numbers than they could achieve because it is nearly always desirable
1196 in a DNS study to maximize Reynolds number. An alternative explanation is that ABL
1197 LES users frequently run ensembles to examine a particular hypothesis (e.g., sensi-
1198 tivity of a physical process to large-scale forcing) limiting their available maximum
1199 number of grid points. To explore this, the number of ensemble members at the max-
1200 imum number of grid points was recorded for each paper as well as the total number
1201 of prognostic variables used in the simulation to examine if physical complexity con-

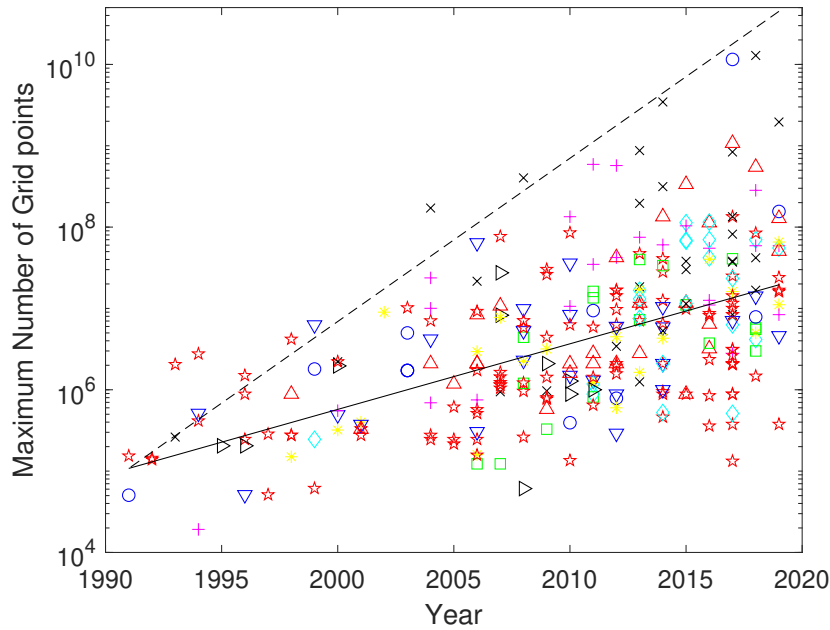


Fig. 4 Maximum number of grid points used in LES published in BLM in each year since 1990. The solid line corresponds to a best fit power law of $2^{0.27}$ and the dashed line to the theoretical value of $2^{0.67}$

1202 tributes to the decreased scaling exponent. The scaling exponent calculated from the
 1203 product of the maximum number of grid points, the number of prognostic variables,
 1204 and the number of ensemble members is only slightly larger (0.29) than that for only
 1205 the maximum number of grid points a strong counter to this explanation.

1206 A third possibility is that the lower exponent is indicative of resource limitations.
 1207 Researchers would run with more grid points but they do not have access to the re-
 1208 quired HPC infrastructure or, they do not have the required resources or experience
 1209 to improve their software infrastructure to take full advantage of available HPC. One
 1210 testable hypothesis related to this is that if resource limitations have some explana-
 1211 tory power it would manifest through different trends in different countries as a result
 1212 of disparities in funding levels and or the effectiveness of different funding systems
 1213 (e.g., Sandström and Van den Besselaar 2018). Country of origin was assumed to be
 1214 the country of the corresponding author. To enable trend detection, countries with-
 1215 out sufficient numbers of papers attributed to them were grouped. The grouping was
 1216 loosely done by region under the assumption that resources were more likely than not
 1217 to be similar in a geographic region.

1218 When the scaling plot is broken down by country, some trends can be discerned.
 1219 First, it is evident that the majority of the simulations since 2004 that achieve the
 1220 theoretical scaling have an origin in Germany. This is only a short time after the intro-
 1221 duction of the parallelized LES model (PALM, Raasch and Schröter 2001). A second

Table 1 Number of articles identified for each country or region group and the corresponding symbol used in Figure 4

Countries	Number of Articles	Symbol
Australia, Malaysia, New Zealand, Singapore, Korea	12	○
China	17	□
Japan	23	+
Belgium, Croatia, Denmark, Finland, Italy, Norway, Poland, Portugal, Spain, Sweden	28	△
Netherlands, Switzerland	21	◇
Germany	28	x
France	20	*
England	25	▽
Brazil, Canada	10	▷ψ
United States	104	☆

1222 observation is that although many of the initial simulations that are close to the the-
 1223 oretical line are from groups in the United States and England, after 2007 we see a
 1224 reduction in the maximum number of grid points from these two countries. Because
 1225 simulations from only one journal are included in the analysis, it is difficult to take
 1226 this as more than an indicator that further inquiry is merited.

1227 4.2 The *Terra-Incognita* in large-eddy simulations

1228 A fundamental pillar of LES is the filtering operation at scale Δ that enables partial
 1229 resolution of turbulent eddies, and requires modeling of the smaller unresolved ones
 1230 (Lilly 1967). If Δ is of similar order to the Kolmogorov scale, the limit of DNS is
 1231 reached. Alternatively, if filtering takes place beyond the inertial regime, at scales
 1232 larger or similar to the turbulence integral length-scale (l_i) the limit of RANS is ap-
 1233 proached. When the former limit is asymptotically approached, the corresponding
 1234 contribution of the subgrid-scale terms are small, especially in regions far from solid
 1235 objects, or interfaces. As a result, the progressive evolution of LES towards DNS only
 1236 hinges on the continuous development of faster and more capable computers (e.g.,
 1237 Fig. 4). Much to the contrary, in the latter limit where filtering occurs at very large
 1238 scales –i.e. in the vicinity of the local turbulence integral scale ($l_i/\Delta \sim 1$), the so-
 1239 called ‘*Terra-Incognita*’ region or ‘gray zone’ is reached (Wyngaard 2004; Honnert
 1240 et al. 2020), where the conceptual basis on which current LES subgrid-scale modelling
 1241 stands crumbles. This challenging limit is traditionally the fringe region between the
 1242 realm of numerical weather predictions (based on a RANS approach) and LES, and
 1243 thus happens to be the region where most publications in ABL flows are developed.

1244 The backbone of LES is K-41, which predicts the existence of an inertial regime
 1245 where TKE is not generated, nor destroyed, but simply transferred through an eddy
 1246 cascade. This *a priori* simplistic transfer of energy from bigger to smaller turbulent
 1247 eddies provides a window of opportunity for models, which besides the traditional
 1248 physical constraints of Galilean mechanics (Pope 2000), only have to ensure the ap-
 1249 propriate transfer of energy. The challenge arises when filtering occurs at scales either
 1250 too close to the inertial limit, or beyond, given that flow dynamics in this region can be
 1251 dominated by strong non-linear interactions between the mean flow and turbulence.

1252 More specifically, at these large scales TKE is no longer simply transferred, but tur-
1253 bulence can actively interact with the mean flow, potentially leading to an additional
1254 generation or destruction of TKE. This additional non-linear interaction will further
1255 dictate the extent of the TKE's inertial regime. Furthermore, at these large scales there
1256 can also exist a backscatter of TKE from the turbulent eddies into the mean flow,
1257 which is not well predicted by K-41's theory, and hence missed in most SGS models.
1258 Therefore, the term of '*Terra-Icognita*' introduced in Wyngaard (2004), refers to the
1259 limit $l_i/\Delta \sim 1$, where neither LES nor mesoscale modeling were designed to operate.
1260 This limit represents an important challenge in developing multi-resolution models
1261 than can dynamically evolve from an LES to a RANS approach, as it is desired in
1262 most modeling of atmospheric flows and the theoretical limit of the '*Terra-Icognita*',
1263 is not a static limit to be addressed by adjusting the numerical resolution of the com-
1264 putational model, but instead should be considered through the glasses of a dynamical
1265 system. This is because a flow that can *a priori* be properly resolved, can progressively
1266 evolve as a result of external forcings towards the '*Terra-Icognita*' limit (Heerwaar-
1267 den et al. 2014; Margairaz et al. 2020b,a). For example, consider a turbulent flow with
1268 initial characteristic l_{iw} that is being integrated with a fixed RANS grid resolution Δ
1269 such that $l_i/\Delta \ll \mu$. At a later stage, due to external surface complexities (e.g. het-
1270 erogeneous surface heating, changes in roughness, etc.), large-flow perturbations can
1271 develop such that now $l_i/\Delta \sim 1$. While initially the flow was well captured with the
1272 RANS approach, at the later stage this would fail to appropriately represent the flow
1273 physics because the simulation entered the '*Terra-Icognita*' region. A similar argu-
1274 ment can be observed from the LES reference frame, if one for example considers a
1275 case where while initially $l_i/\Delta \gg 1$, the simulation evolves towards a scenario where
1276 $l_i/\Delta \sim 1$ as a result of a reduction in l_i . This is the case for example in transitional
1277 BLs, going from unstable to stable stratification, where submeso motions can play a
1278 very important role (Sun et al. 2004; Mahrt and Thomas 2016).

1279 At present the limitation of LES for poorly resolved large scales is the fact that
1280 there exists no theory that can universally predict the bijective interaction between
1281 the mean flow and unresolved, energy-containing eddies since this is case-to-case
1282 dependent, as expressed by the *a-priori* neglected non-linear terms in the tendency
1283 equation for the mean shear stress in almost all models (Wyngaard 2004). Despite
1284 these challenges, researchers continue to use LES as a tool to develop and evaluate
1285 scale-aware parameterization schemes that can be applicable to weather models at
1286 grey-zone resolutions (Shin and Hong 2015; Shin and Dudhia 2016; Margairaz et al.
1287 2020a). Nonetheless, the transition from RANS to LES simulations in an accurate,
1288 physics-based approach, remains a research chimera with the promise of great-gain
1289 and high-reward.

1290 4.3 What is Next?

1291 Over the last 50 years, the LES technique has gone from an emerging computational
1292 methodology to one of the major ways that researchers study the ABL. From its orig-
1293 inal roots studying simple channel flows and CBLs (Deardorff 1970a, 1972a), LES
1294 now covers all the primary application areas that ABL researchers explore. The tech-

1295 nique itself has matured through a strong focus on theory, model development, and
1296 validation studies to the point where researchers trust it to provide insight into a wide
1297 range of turbulent phenomena in the ABL.

1298 We surveyed six application areas where LES has been extensively applied to
1299 understand the performance of the technique and to study the physics of turbulent
1300 transport and its impact on the application of interest. These areas include the con-
1301 vective boundary layer, the stable boundary layer, transitional boundary layers, plant
1302 canopy flows, urban flows and dispersion, and land-surface heterogeneity. In each
1303 area, a common theme can be identified. Applications begin by adding any additional
1304 physics missing from prior studies and then they examine the validity of the LES tech-
1305 nique and refine deficient models. Although this cycle of development does not ever
1306 completely end, after it is mature researchers in a given application area move towards
1307 ever more complex case studies aimed at increasing the realism of simulations. The
1308 increasing complexity has allowed researchers to widen their understanding of ABL
1309 fluxes of momentum and scalars and turn the LES technique into a tool that comple-
1310 ments inquires using theory and laboratory and field experiments.

1311 When we think about what the next frontiers are for ABL LES we can identify
1312 a few areas. One is further model development, including SGS models when energy
1313 containing length scales are poorly resolved in the ‘*Terra-Icognita*’ (e.g., strong strati-
1314 fication without extreme resolution) and especially for surface boundary conditions. In
1315 nearly all flows with the exception of dense plant canopies, boundary conditions at the
1316 land (or building) surface play a critical role in the exchange of momentum, heat, and
1317 moisture between the land surface and the atmosphere and ultimately in ABL dynam-
1318 ics. Even though this is well known, most modeling efforts use equilibrium models
1319 (Eq. 9) with a poor description of the land surface. Efforts to develop better models
1320 have been progressing including those that attempt to improve the representation of
1321 unresolved features (Anderson and Meneveau 2011) and non-equilibrium models that
1322 use the integral form of the boundary layer equations (Yang et al. 2015). Yet general
1323 models that can address the wide range of surface and atmospheric conditions found
1324 in the ABL are still needed. This includes the impacts of local advection, stratifica-
1325 tion, and slope. In particular, proper LES surface boundary conditions for slope flows
1326 basically do not exist.

1327 Another frontier is the continued march towards more realistic forcing, domains,
1328 boundary conditions, and physical descriptions. As computing power has increased,
1329 researchers in all the application areas continue to push towards conditions that more
1330 closely match those observed in the ABL. This has been enabled by the continued
1331 growth in computational power (e.g., Fig. 4), a need for better knowledge of the
1332 physics of the ABL, and a desire to move towards predictive LES. Researchers have al-
1333 ready used the available computational power to address questions that are intractable
1334 in any other way. Although not reviewed here, an early example comes from the cloud
1335 modeling community where very large domain simulations have enabled the study of
1336 deep tropical convection and its impact on cloud formation, a critical component to-
1337 ward improving the representation of clouds in global climate models (Khairoutdinov
1338 et al. 2009). More recently, (Dipankar et al. 2015; Heinze et al. 2017) have explored
1339 the ability of LES to resolve convection and cloud processes at a spatial extent that
1340 covered all of Germany. Although the model was coarse for LES and used a simple

1341 SGS model, comparisons to data were satisfactory. Other researchers have shown that
1342 it is not only possible to simulate large domains but that long time integrations can
1343 also be done (Schalkwijk et al. 2016).

1344 These efforts and others indicate that a path towards predictive LES of near surface
1345 processes is possible. Using the fits depicted in Fig. 4, we can estimate when we might
1346 be able to carry out LES with sufficient resolution to resolve diurnal ABL processes
1347 (e.g., not just convection) and large enough extent to be relevant to mesoscale weather.
1348 Based on work examining moderately stratified SBLs (Beare et al. 2006; Sullivan et al.
1349 2016) a grid resolution $\Delta \approx 10$ m is sufficient to nominally resolve terrain and SBL
1350 features. If we further assume a vertical domain extent of 5 km would start to capture
1351 mesoscale weather features, numerical codes that achieve scaling at the theoretical
1352 limit would be able to simulate a horizontal domain the size of a mid-sized state in the
1353 western United States (e.g., Utah) or a mid sized country in Europe (e.g., the United
1354 Kingdom) in around 2026. While this is encouraging, when the average scaling is
1355 used the soonest you would expect similar simulation would be 2078. If we extend to
1356 horizontal domains on the order of the entire United States (or approximately Europe),
1357 this is at best possible in 2035 and following the average scaling in 2099.

1358 Many barriers still exist to LES becoming a tool that can be used to study the full
1359 range of ABL physics and even move on to becoming a predictive modelling tool.
1360 These include improved models and boundary conditions that can adapt to the wide
1361 range of possible surface conditions, continued improvements to lateral coupling with
1362 coarser scale models (e.g., Muñoz-EsTarza et al. 2014; Rai et al. 2019), and more
1363 work to generate the knowledge and understanding of the ‘*Terra-Incognita*’ region,
1364 so coupling of multi-resolution models becomes physics based instead of current ad-
1365 hoc approaches. In addition, higher resolution of ABL processes and land-atmosphere
1366 coupling will require continued improvements to our description of the land surface
1367 itself. Advancements in thermal and LiDAR remote sensing are hopeful paths to this
1368 (e.g., Kustas and Anderson 2009; Liu et al. 2017) but significant work is still required
1369 to turn the information these techniques provide into the surface descriptions that sim-
1370 ulations need. Lastly, for these goals to be broadly met by researchers more simulation
1371 codes will need software infrastructure upgrades and ABL researchers will need con-
1372 tinued and improved access to high performance computing hardware.

1373 **Acknowledgements** This research was supported by the National Science Foundation grants AGS-1660367
1374 (R. Stoll and J. Gibbs) and PDM-1649067 and PDM-1712538 (M. Calaf) and the NOAA/Office of Oceanic
1375 and Atmospheric Research under NOAA–University of Oklahoma Cooperative Agreement NA11OAR4320072,
1376 U.S. Department of Commerce (J. Gibbs).

1377 References

1378 Ackerman AS, vanZanten MC, Stevens B, Savic-Jovicic V, Bretherton CS, Chlond A,
1379 Golaz JC, Jiang H, Khairoutdinov M, Krueger SK, Lewellen DC, Lock A, Moeng
1380 CH, Nakamura K, Petteers MD, Snider JR, Weinbrecht S, Zulauf M (2009) Large-
1381 Eddy Simulations of a Drizzling, Stratocumulus-Topped Marine Boundary Layer.
1382 *Mon Wea Rev* 137(3):1083–1110, DOI 10.1175/2008MWR2582.1

- 1383 Adrian RJ, Meinhart CD, Tomkins CD (2000) Vortex organization in the outer region
1384 of the turbulent boundary layer. *J Fluid Mech* 422:1–54
- 1385 Albertson JD, Kustas WP, Scanlon TM (2001) Large-eddy simulation over hetero-
1386 geneous terrain with remotely sensed land surface conditions. *Water Resour Res*
1387 37(7):1939–1953
- 1388 Anderson R, Meneveau C (1999) Effects of the similarity model in finite-difference
1389 LES of isotropic turbulence using a Lagrangian dynamic mixed model. *Flow Turbul*
1390 *Combust* 62(3):201–225
- 1391 Anderson W (2012) An immersed boundary method wall model for high-Reynolds
1392 number channel flow over complex topography. *Int J Numer Methods Fluids*
1393 71:1588–1608
- 1394 Anderson W (2019a) A15–1–15. *J Fluid Mech* 869:27–84
- 1395 Anderson W (2019b) Non-periodic phase-space trajectories of roughness-driven sec-
1396 ondary flows in high- re_{τ} boundary layers and channels. *J Fluid Mech* 869:27–84
- 1397 Anderson W, Meneveau C (2010) A large-eddy simulation model for boundary-layer
1398 flow over surfaces with horizontally resolved but vertically unresolved roughness
1399 elements. *Boundary-Layer Meteorol* 137:397–415
- 1400 Anderson W, Meneveau C (2011) Dynamic roughness model for large-eddy simu-
1401 lation of turbulent flow over multiscale, fractal-like rough surfaces. *J Fluid Mech*
1402 679:288–314
- 1403 Anderson W, Barros J, Christensen K, Awasthi A (2015) Numerical and experimental
1404 study of mechanisms responsible for turbulent secondary flows in boundary layer
1405 flows over spanwise heterogeneous roughness. *J Fluid Mech* 768:316–347
- 1406 Andren A (1995) The structure of stably stratified atmospheric boundary layers: A
1407 large-eddy simulation study. *Quart J Roy Meteor Soc* 121(525):961–985
- 1408 Andren A, Brown AR, Mason PJ, Graf J, Schumann U, Moeng CH, Nieuwstadt FT
1409 (1994) Large-eddy simulation of a neutrally stratified boundary layer: A compari-
1410 son of four computer codes. *Quart J Roy Meteor Soc* 120(520):1457–1484
- 1411 Antonia R, Luxton R (1971) The response of a turbulent boundary layer to a step
1412 change in surface roughness part i. smooth to rough. *J Fluid Mech* 48:721–761
- 1413 Armenio V, Sarkar S (2002) An investigation of stably stratified turbulent channel
1414 flow using large-eddy simulation. *J Fluid Mech* 459:1–42
- 1415 Aumond P, Masson V, Lac C, Gauvreau B, Dupont S, Berengier M (2013) Including
1416 the drag effects of canopies: Real case large-eddy simulation studies. *Boundary-*
1417 *Layer Meteorol* 146(1):65–80
- 1418 Avissar R, Schmidt T (1998) An evaluation of the scale at which ground-
1419 surface heat flux patchiness affects the convective boundary layer using
1420 large-eddy simulations. *J Atmos Sci* 55(16):2666–2689, DOI 10.1175/1520-
1421 0469(1998)055<2666:AEOTSA>2.0.CO;2
- 1422 Ayotte KW, Sullivan PP, Andren A, Doney SC, Holtslag AA, Large WG, McWilliams
1423 JC, Moeng CH, Otte MJ, Tribbia JJ, et al. (1996) An evaluation of neutral and con-
1424 vective planetary boundary-layer parameterizations relative to large eddy simula-
1425 tions. *Boundary-Layer Meteorol* 79(1-2):131–175
- 1426 Baidya Roy S, Avissar R (2000) Scales of response of the convective boundary layer
1427 to land-surface heterogeneity. *Geophys Res Lett* 27(4):533–536

- 1428 Bailey BN, Stoll R (2013) Turbulence in sparse, organized vegetative canopies: a
1429 large-eddy simulation study. *Boundary-Layer Meteorol* 147:369–400, DOI DOI
1430 10.1007/s10546-012-9796-4
- 1431 Bailey BN, Stoll R (2016) The creation and evolution of coherent structures in plant
1432 canopy flows and their role in turbulent transport. *J Fluid Mech* 789:425–460
- 1433 Bailey BN, Stoll R, Pardyjak ER, Mahaffee WF (2014) Effect of vegetative canopy
1434 architecture on vertical transport of massless particles. *Atmos Environ* 95:480–489
- 1435 Baker J, Walker HL, Cai X (2004) A study of the dispersion and transport of reactive
1436 pollutants in and above street canyons—a large eddy simulation. *Atmos Environ*
1437 38(39):6883–6892
- 1438 Bao J, Chow F, Lundquist K (2018) Large-eddy simulation over complex terrain using
1439 an improved immersed boundary method in the weather research and forecasting
1440 mode. *Mon Wea Rev* 146:2781–2797
- 1441 Bardina J, Ferziger J, Reynolds W (1980) Improved subgrid-scale models for large-
1442 eddy simulation. In: 13th Fluid and Plasma Dynamics Conference, pp 1–9, DOI
1443 10.2514/6.1980-1357
- 1444 Basu S, Lacser A (2017) A cautionary note on the use of Monin–Obukhov similarity
1445 theory in very high-resolution large-eddy simulations. *Boundary-Layer Meteorol*
1446 163(2):351–355
- 1447 Basu S, Porté-agel F, Foufoula-Georgiou E, Vinuesa JF, Pahlow M (2006) Revisiting
1448 the local scaling hypothesis in stably stratified atmospheric boundary-layer turbu-
1449 lence: an integration of field and laboratory measurements with large-eddy simu-
1450 lations. *Boundary-Layer Meteorol* 119(3):473–500, DOI 10.1007/s10546-005-9036-
1451 2
- 1452 Basu S, Holtslag AA, Van De Wiel BJ, Moene AF, Steeneveld GJ (2008a) An incon-
1453 venient “truth” about using sensible heat flux as a surface boundary condition in
1454 models under stably stratified regimes. *Acta Geophys* 56(1):88–99
- 1455 Basu S, Vinuesa JF, Swift A (2008b) Dynamic LES modeling of a diurnal cycle. *J*
1456 *Appl Meteor Climatol* 47(4):1156–1174
- 1457 Beare RJ (2008) The role of shear in the morning transition boundary layer. *Boundary-*
1458 *Layer Meteorol* 129(3):395–410
- 1459 Beare RJ, Macvean MK, Holtslag AA, Cuxart J, Esau I, Golaz JC, Jimenez MA,
1460 Khairoutdinov M, Kosovic B, Lewellen D, Lund TS, Lundquist JK, McCabe A,
1461 Moene AF, Noh Y, Raasch S, Sullivan P (2006) An intercomparison of large-eddy
1462 simulations of the stable boundary layer. *Boundary-Layer Meteorol* 118(2):247–
1463 272
- 1464 Belcher S, Harman I, Finnigan J (2012) The wind in the willows: flows in forest
1465 canopies in complex terrain. *Annu Rev Fluid Mech* 44:479–504
- 1466 Bohrer G, Katul GG, Walko RL, Avissar R (2009) Exploring the effects of microscale
1467 structural heterogeneity of forest canopies using large-eddy simulations. *Boundary-*
1468 *Layer Meteorol* 132(3):351–382
- 1469 Boppa V, Xie ZT, Castro IP (2010) Large-eddy simulation of dispersion from sur-
1470 face sources in arrays of obstacles. *Boundary-Layer Meteorol* 135(3):433–454
- 1471 Boppa V, Xie ZT, Castro IP (2014) Thermal stratification effects on flow over a
1472 generic urban canopy. *Boundary-Layer Meteorol* 153(1):141–162

- 1473 Bou-Zeid E (2015) Challenging the large eddy simulation technique with advanced a
1474 posteriori tests. *J Fluid Mech* 764:1–4
- 1475 Bou-Zeid E, Meneveau C, Parlange M (2004) Large-eddy simulation of neutral at-
1476 mospheric boundary layer flow over heterogeneous surfaces: Blending height and
1477 effective surface roughness. *Water Resour Res* 40:W02,505
- 1478 Bou-Zeid E, Meneveau C, Parlange M (2005) A scale-dependent Lagrangian dy-
1479 namic model for large eddy simulation of complex turbulent flows. *Phys Fluids*
1480 17(2):025,105, DOI 10.1063/1.1839152
- 1481 Bou-Zeid E, Parlange M, Meneveau C (2007) On the parameterization of surface
1482 roughness at regional scales. *J Atmos Sci* 64:216–227
- 1483 Bou-Zeid E, Overney J, Rogers BD, Parlange MB (2009) The effects of building rep-
1484 resentation and clustering in large-eddy simulations of flows in urban canopies.
1485 *Boundary-Layer Meteorol* 132(3):415–436
- 1486 Boudreault LÉ, Dupont S, Bechmann A, Dellwik E (2017) How forest inhom-
1487 ogeneities affect the edge flow. *Boundary-Layer Meteorol* 162(3):375–400
- 1488 Brown AR, Derbyshire S, Mason PJ (1994) Large-eddy simulation of stable atmo-
1489 spheric boundary layers with a revised stochastic subgrid model. *Quart J Roy Me-
1490 teor Soc* 120(520):1485–1512
- 1491 Brutsaert W (1982) *Evaporation into the Atmosphere*. Kluwer Academic Publishers,
1492 Norwell, MA
- 1493 Cai XM (2012) Effects of wall heating on flow characteristics in a street canyon.
1494 *Boundary-Layer Meteorol* 142(3):443–467
- 1495 Cai XM, Barlow J, Belcher S (2008) Dispersion and transfer of passive scalars in and
1496 above street canyons—large-eddy simulations. *Atmos Environ* 42(23):5885–5895
- 1497 Carper MA, Porté-Agel F (2004) The role of coherent structures in subfilter-scale
1498 dissipation of turbulence measured in the atmospheric surface layer. *J Turbul* 5:32–
1499 32
- 1500 Carper MA, Porté-Agel F (2008) Subfilter-scale fluxes over a surface roughness tran-
1501 sition. part ii: A priori study of large-eddy simulation models. *Boundary-Layer Me-
1502 teorol* 127(1):73–95
- 1503 Cassiani M, Katul G, Albertson J (2008) The effects of canopy leaf area index on air-
1504 flow across forest edges: Large-eddy simulation and analytical results. *Boundary-
1505 Layer Meteorol* 126(3):433–460
- 1506 Castagnera K, Cheng D, Fatoohi R, Hook E, Kramer B, Manning C, Musch J, Niggley
1507 C, Saphir W, Sheppard D, et al. (1994) Clustered workstations and their potential
1508 role as high speed compute processors. *NAS Computational Services Technical
1509 Report RNS-94-003*, NAS Systems Division, NASA Ames Research Center
- 1510 Castro IP (2017) Are urban-canopy velocity profiles exponential? *Boundary-Layer
1511 Meteorol* 164(3):337–351
- 1512 Chester S, Meneveau C, Parlange M (2007) Modelling of turbulent flow over fractal
1513 trees with renormalized numerical simulation. *J Comp Phys* 225:427–448
- 1514 Chow FK, Street RL, Xue M, Ferziger JH (2005) Explicit filtering and reconstruction
1515 turbulence modeling for large-eddy simulation of neutral boundary layer flow. *J
1516 Atmos Sci* 62(7):2058–2077
- 1517 Clark T (1977) A small-scale dynamic model using terrain-following coordinate trans-
1518 formation. *J Comp Phys* 24:186–215

- 1519 Colwell RP (2019) How we made the pentium processors. *Nat Electron* 2(2):83–84
- 1520 Conzemius RJ, Fedorovich E (2006) Dynamics of sheared convective boundary layer
1521 entrainment. part i: Methodological background and large-eddy simulations. *J At-*
1522 *mos Sci* 63(4):1151–1178
- 1523 Courault D, Drobinski P, Brunet Y, Lacarrere P, Talbot C (2007) Impact of sur-
1524 face heterogeneity on a buoyancy-driven convective boundary layer in light winds.
1525 *Boundary-Layer Meteorol* 124(3):383–403
- 1526 Cui Z, Cai X, J Baker C (2004) Large-eddy simulation of turbulent flow in a street
1527 canyon. *Quart J Roy Meteor Soc* 130(599):1373–1394
- 1528 Cuxart J, Holslag AA, Beare RJ, Bazile E, Beljaars A, Cheng A, Conangla L, Ek M,
1529 Freedman F, Hamdi R, Kerstein H, Kitagawa G, Lenderink D, Lewellen J, Mailhot
1530 T, Mauritsen V, Perov G, Schayes GJ, Steeneveld GS, Taylor P, Weng W, Wun-
1531 sch S, Xu KM (2006) Single-column model intercomparison for a stably stratified
1532 atmospheric boundary layer. *Boundary-Layer Meteorol* 118(2):273–303
- 1533 Deardorff JW (1970a) A numerical study of three-dimensional turbulent chan-
1534 nel flow at large reynolds numbers. *J Fluid Mech* 41(2):453–480, DOI
1535 10.1017/S0022112070000691
- 1536 Deardorff JW (1970b) Preliminary results from numerical integrations of the unstable
1537 planetary boundary layer. *J Atmos Sci* 27(8):1209–1211
- 1538 Deardorff JW (1971) On the magnitude of the subgrid scale eddy coefficient. *J Comp*
1539 *Phys* 7(1):120–133, DOI [https://doi.org/10.1016/0021-9991\(71\)90053-2](https://doi.org/10.1016/0021-9991(71)90053-2)
- 1540 Deardorff JW (1972a) Numerical investigation of neutral and unstable
1541 planetary boundary layers. *J Atmos Sci* 29:91–115, DOI 10.1175/1520-
1542 0469(1972)029<0091:nionau>2.0.co;2
- 1543 Deardorff JW (1972b) Theoretical expression for the countergradient vertical heat
1544 flux. *J Geophys Res* 77(30):5900–5904
- 1545 Deardorff JW (1973) The use of subgrid transport equations in a three-
1546 dimensional model of atmospheric turbulence. *J Fluids Eng* 95(3):429–438, DOI
1547 10.1115/1.3447047, URL <https://doi.org/10.1115/1.3447047>
- 1548 Deardorff JW (1974a) Three-dimensional numerical study of the height and mean
1549 structure of a heated planetary boundary layer. *Boundary-Layer Meteorol* 7(1):81–
1550 106
- 1551 Deardorff JW (1974b) Three-dimensional numerical study of turbulence in an entrain-
1552 ing mixed layer. *Boundary-Layer Meteorol* 7(2):199–226
- 1553 Deardorff JW (1980) Stratocumulus-capped mixed layers derived from a
1554 three-dimensional model. *Boundary-Layer Meteorol* 18:495–527, DOI
1555 10.1007/BF00119502
- 1556 Dipankar A, Stevens B, Heinze R, Moseley C, Zängl G, Giorgetta M, Brdar S (2015)
1557 Large eddy simulation using the general circulation model ICON. *J Adv Model*
1558 *Earth Syst* 7(3):963–986
- 1559 Dörnbrack A, Schumann U (1993) Numerical simulation of turbulent convective
1560 flow over wavy terrain. *Boundary-Layer Meteorol* 65(4):323–355, DOI
1561 10.1007/BF00707032
- 1562 Dupont S, Brunet Y (2008) Edge flow and canopy structure: a large-eddy simulation
1563 study. *Boundary-Layer Meteorol* 126(1):51–71

- 1564 Dupont S, Gosselin F, Py C, De Langre E, Hemon P, Brunet Y (2010) Modelling
1565 waving crops using large-eddy simulation: Comparison with experiments and a
1566 linear stability analysis. *J Fluid Mech* 652:5–44
- 1567 Dwyer MJ, Patton EG, Shaw RH (1997) Turbulent kinetic energy budgets from a
1568 large-eddy simulation of airflow above and within a forest canopy. *Boundary-Layer
1569 Meteorol* 84(1):23–43
- 1570 Ebert EE, Schumann U, Stull RB (1989) Nonlocal turbulent mixing in the convective
1571 boundary layer evaluated from large-eddy simulation. *J Atmos Sci* 46(14):2178–
1572 2207
- 1573 Fedorovich E, Conzemius R, Esau I, Chow FK, Lewellen D, Moeng CH, Sullivan
1574 P, Pino D, de Arellano JVG (2004) Entrainment into sheared convective boundary
1575 layers as predicted by different large eddy simulation codes. In: 16th Symp. on
1576 Boundary Layers and Turbulence, Portland, ME, Amer. Meteor. Soc. P, p P4.7
- 1577 Fenger J (1999) Urban air quality. *Atmos Environ* 33(29):4877–4900
- 1578 Finnigan J (2000) Turbulence in plant canopies. *Annu Rev Fluid Mech* 32(1):519–571
- 1579 Finnigan JJ, Shaw RH, Patton EG (2009) Turbulence structure above a vegetation
1580 canopy. *J Fluid Mech* 637:387–424
- 1581 Fitzmaurice L, Shaw RH, Paw U KT, Patton EG (2004) Three-dimensional scalar mi-
1582 crofront systems in a large-eddy simulation of vegetation canopy flow. *Boundary-
1583 Layer Meteorol* 112(1):107–127
- 1584 Gal-Chen T, Somerville R (1975) On the use of a coordinate transformation for the
1585 solution of the Navier–Stokes equations. *J Comp Phys* 17:209–228
- 1586 Galmarini S, Beets C, Duynkerke PG, Vila-Guerau de Arellano J (1998) Stable nocturnal
1587 boundary layers: a comparison of one-dimensional and large-eddy simulation
1588 models. *Boundary-Layer Meteorol* 88(2):181–210
- 1589 Gao W, Shaw RH, Paw U KT (1989) Observation of organized structure in turbulent
1590 flow within and above a forest canopy. *Boundary-Layer Meteorol* 47(1):349–377,
1591 DOI 10.1007/BF00122339, URL <https://doi.org/10.1007/BF00122339>
- 1592 Garratt J (1990) The internal boundary layer – a review. *Boundary-Layer Meteorol*
1593 40:171–203
- 1594 Garratt JR (1992) *The Atmospheric Boundary Layer*. Cambridge University Press,
1595 Cambridge, New York
- 1596 Germano M, Piomelli U, Moin P, Cabot WH (1991) A dynamic subgrid-scale eddy
1597 viscosity model. *Phys Fluids A* 3(7):1760–1765, DOI 10.1063/1.857955
- 1598 Geurts BJ (2003) *Elements of Direct and Large Eddy Simulation*. RT Edwards, Inc
- 1599 Ghosal S, Lund TS, Moin P, Akselvoll K (1995) A dynamic localization model
1600 for large-eddy simulation of turbulent flows. *J Fluid Mech* 286:229–255, DOI
1601 10.1017/S0022112095000711
- 1602 Giacomini B, Giometto MG (2020) On the suitability of general-purpose finite-
1603 volume-based solvers for the simulation of atmospheric-boundary-layer flow.
1604 *Geosci Model Dev Discuss* pp 1–28
- 1605 Gibbs JA, Fedorovich E (2014a) Comparison of convective boundary layer velocity
1606 spectra retrieved from large-eddy-simulation and weather research and forecasting
1607 model data. *J Appl Meteor Climatol* 53:377–394, DOI 10.1175/jamc-d-13-033.1
- 1608 Gibbs JA, Fedorovich E (2014b) Effects of temporal discretization on turbu-
1609 lence statistics and spectra in numerically simulated convective boundary layers.

- 1610 Boundary-Layer Meteorol 153:19–41, DOI 10.1007/s10546-014-9936-0
- 1611 Gibbs JA, Fedorovich E (2016) Sensitivity of turbulence statistics in the lower portion
1612 of a numerically simulated stable boundary layer to parameters of the Deardorff
1613 subgrid turbulence model. *Quart J Roy Meteor Soc* 142(698):2205–2213
- 1614 Gibbs JA, Fedorovich E, Shapiro A (2015) Revisiting surface heat-flux and tem-
1615 perature boundary conditions in models of stably stratified boundary-layer flows.
1616 *Boundary-Layer Meteorol* 154(2):171–187
- 1617 Giometto M, Christen A, Meneveau C, Fang J, Krafczyk M, Parlange M (2016) Spa-
1618 tial characteristics of roughness sublayer mean flow and turbulence over a realistic
1619 urban surface. *Boundary-Layer Meteorol* 160(3):425–452
- 1620 Giometto MG, Christen A, Egli PE, Schmid M, Tooke R, Coops N, Parlange MB
1621 (2017) Effects of trees on mean wind, turbulence and momentum exchange within
1622 and above a real urban environment. *Adv Water Resour* 106:154–168
- 1623 Grimmond C, Oke TR (1999) Aerodynamic properties of urban areas derived from
1624 analysis of surface form. *J Appl Meteor* 38(9):1262–1292
- 1625 Grinstein FF, Margolin LG, Rider WJ (2007) *Implicit Large Eddy Simulation*, vol 10.
1626 Cambridge University Press Cambridge
- 1627 Gropp W, Lusk E, Doss N, Skjellum A (1996) A high-performance, portable im-
1628 plementation of the MPI message passing interface standard. *Parallel Comput*
1629 22(6):789–828
- 1630 Hadfield MG, Cotton WR, Pielke RA (1992) Large-Eddy Simulations of Thermally
1631 Forced Circulations in the Convective Boundary Layer. Part II: The Effect of
1632 Changes in Wavelength and Wind Speed. *Boundary-Layer Meteorol* 58:307–327
- 1633 Hanna S, Tehranian S, Carissimo B, Macdonald R, Lohner R (2002) Comparisons of
1634 model simulations with observations of mean flow and turbulence within simple
1635 obstacle arrays. *Atmos Environ* 36(32):5067–5079
- 1636 Hayati AN, Stoll R, Pardyjak ER, Harman T, Kim J (2019) Comparative metrics
1637 for computational approaches in non-uniform street-canyon flows. *Build Environ*
1638 158:16–27
- 1639 Hechtel LM, Stul RB, Moeng CH (1990) The effects of nonhomogeneous
1640 surface fluxes on the convective boundary layer: A case study using
1641 large-eddy simulation. *J Atmos Sci* 47(14):1721–1741, DOI 10.1175/1520-
1642 0469(1990)047<1721:TEONSF>2.0.CO;2
- 1643 Heerwaarden CCv, Mellado JP, Lozar AD (2014) Scaling laws for the heteroge-
1644 neously heated free convective boundary layer. *J Atmos Sci* 71(11):3975–4000,
1645 DOI 10.1175/jas-d-13-0383.1
- 1646 Heinze R, Dipankar A, Henken CC, Moseley C, Sourdeval O, Trömel S, Xie X,
1647 Adamidis P, Ament F, Baars H, et al. (2017) Large-eddy simulations over Germany
1648 using ICON: A comprehensive evaluation. *Quart J Roy Meteor Soc* 143(702):69–
1649 100
- 1650 Hildebrand PH, Ackerman B (1984) Urban effects on the convective boundary layer.
1651 *J Atmos Sci* 41(1):76–91
- 1652 Hinze JO (1967) Secondary currents in wall turbulence. *Phys Fluids* 10(9):S122–
1653 S125, DOI 10.1063/1.1762429
- 1654 Holtslag A, Moeng CH (1991) Eddy diffusivity and countergradient transport in the
1655 convective atmospheric boundary layer. *J Atmos Sci* 48(14):1690–1698

- 1656 Holtslag A, Svensson G, Baas P, Basu S, Beare B, Beljaars A, Bosveld F, Cuxart
1657 J, Lindvall J, Steeneveld G, et al. (2013) Stable atmospheric boundary layers and
1658 diurnal cycles: Challenges for weather and climate models. *Bull Amer Meteor Soc*
1659 94(11):1691–1706
- 1660 Honnert R, Efstathiou GA, Beare RJ, Ito J, Lock A, Neggers R, Plant RS, Shin
1661 HH, Tomassini L, Zhou B (2020) The atmospheric boundary layer and the “gray
1662 zone” of turbulence: A critical review. *J Geophys Res Atmos* 125(13), DOI
1663 10.1029/2019jd030317
- 1664 Huang HY, Margulis SA (2010) Evaluation of a fully coupled large-eddy simulation–
1665 land surface model and its diagnosis of land-atmosphere feedbacks. *Water Resour*
1666 *Res* 46(6)
- 1667 Huang J, Bou-Zeid E (2013) Turbulence and vertical fluxes in the stable atmospheric
1668 boundary layer. part i: a large-eddy simulation study. *J Atmos Sci* 70(6):1513–1527
- 1669 Huang J, Lee X, Patton EG (2009) Dissimilarity of scalar transport in the con-
1670 vective boundary layer in inhomogeneous landscapes. *Boundary-Layer Meteorol*
1671 130(3):327–345
- 1672 Hutchins N, Marusic I (2007) Evidence of very long meandering features in the log-
1673 arithmic region of turbulent boundary layers. *J Fluid Mech* 579:1–28
- 1674 Hwang H, Lee J (2018) Secondary flows in turbulent boundary layers over longitudi-
1675 nal surface roughness. *Phys Rev Fluids* 3:014,608
- 1676 Jeong J, Hussain F (1995) On the identification of a vortex. *J Fluid Mech* 285:69–94
- 1677 Kanda M (2006) Large-eddy simulations on the effects of surface geometry of
1678 building arrays on turbulent organized structures. *Boundary-Layer Meteorol*
1679 118(1):151–168
- 1680 Kanda M, Hino M (1994) Organized structures in developing turbulent flow within
1681 and above a plant canopy, using a large eddy simulation. *Boundary-Layer Meteorol*
1682 68(3):237–257
- 1683 Kanda M, Inagaki A, Letzel MO, Raasch S, Watanabe T (2004a) LES study of the
1684 energy imbalance problem with eddy covariance fluxes. *Boundary-Layer Meteorol*
1685 110(3):381–404
- 1686 Kanda M, Moriwaki R, Kasamatsu F (2004b) Large-eddy simulation of turbulent
1687 organized structures within and above explicitly resolved cube arrays. *Boundary-*
1688 *Layer Meteorol* 112(2):343–368
- 1689 Kanda M, Inagaki A, Miyamoto T, Gryscha M, Raasch S (2013) A new aerodynamic
1690 parametrization for real urban surfaces. *Boundary-Layer Meteorol* 148(2):357–377
- 1691 Khairoutdinov MF, Krueger SK, Moeng CH, Bogenschutz PA, Randall DA (2009)
1692 Large-eddy simulation of maritime deep tropical convection. *J Adv Model Earth*
1693 *Syst* 1(4)
- 1694 Khan HN, Hounshell DA, Fuchs ER (2018) Science and research policy at the end of
1695 Moore’s law. *Nature Electronics* 1(1):14–21
- 1696 Khanna S, Basseur JG (1997) Analysis of Monin–Obukhov similarity from large-
1697 eddy simulation. *J Fluid Mech* 345:251–286
- 1698 Khanna S, Basseur JG (1998) Three-dimensional buoyancy-and shear-induced local
1699 structure of the atmospheric boundary layer. *J Atmos Sci* 55(5):710–743
- 1700 Kim SW, Park SU, Moeng CH (2003) Entrainment processes in the convective bound-
1701 ary layer with varying wind shear. *Boundary-Layer Meteorol* 108(2):221–245

- 1702 Kolmogorov AN, Levin V, Hunt JCR, Phillips OM, Williams D (1991) The local
1703 structure of turbulence in incompressible viscous fluid for very large Reynolds
1704 numbers. *Proc R Soc Lond A* 434(1890):9–13, DOI 10.1098/rspa.1991.0075
- 1705 Kosović B, Curry JA (2000) A large eddy simulation study of a quasi-steady, stably
1706 stratified atmospheric boundary layer. *J Atmos Sci* 57(8):1052–1068
- 1707 Kröniger K, De Roo F, Brugger P, Huq S, Banerjee T, Zinsser J, Rotenberg E, Yakir
1708 D, Rohatyn S, Mauder M (2018) Effect of secondary circulations on the surface–
1709 atmosphere exchange of energy at an isolated semi-arid forest. *Boundary-Layer
1710 Meteorol* 169(2):209–232
- 1711 Kumar V, Kleissl J, Meneveau C, Parlange MB (2006) Large-eddy simulation of a
1712 diurnal cycle of the atmospheric boundary layer: Atmospheric stability and scaling
1713 issues. *Water Resour Res* 42(6)
- 1714 Kumar V, Svensson G, Holtslag A, Meneveau C, Parlange MB (2010) Impact of sur-
1715 face flux formulations and geostrophic forcing on large-eddy simulations of diurnal
1716 atmospheric boundary layer flow. *J Appl Meteor Climatol* 49(7):1496–1516
- 1717 Kustas W, Anderson M (2009) Advances in thermal infrared remote sensing for land
1718 surface modeling. *Agric For Meteorol* 149(12):2071–2081
- 1719 Kustas WP, Albertson JD (2003) Effects of surface temperature contrast on land-
1720 atmosphere exchange: A case study from Monsoon 90. *Water Resour Res* 39(6)
- 1721 Lemone M (1976) Modulation of turbulence energy by longitudinal rolls in an unsta-
1722 ble planetary boundary layer. *J Atmos Sci* 33(7):1308–1320
- 1723 LeMone MA, Angevine WM, Bretherton CS, Chen F, Dudhia J, Fedorovich E, Kat-
1724 saros KB, Lenschow DH, Mahrt L, Patton EG, et al. (2019) 100 years of progress
1725 in boundary layer meteorology. *Meteorological Monographs* 59:9–1
- 1726 Leonard A (1974) Energy cascade in large-eddy simulations of turbulent fluid flows.
1727 In: *Turbulent Diffusion in Environmental Pollution*, pp 237–248
- 1728 Lesieur M, Métais O, Comte P (2005) *Large-Eddy Simulations of Turbulence*. Cam-
1729 bridge University Press, DOI 10.1017/CBO9780511755507
- 1730 Li Q, Gentine P, Mellado JP, McColl KA (2018) Implications of nonlocal trans-
1731 port and conditionally averaged statistics on Monin–Obukhov similarity theory and
1732 Townsend’s attached eddy hypothesis. *J Atmos Sci* 75(10):3403–3431
- 1733 Li XX, Liu CH, Leung DY (2008) Large-eddy simulation of flow and pollutant dis-
1734 persion in high-aspect-ratio urban street canyons with wall model. *Boundary-Layer
1735 Meteorol* 129(2):249–268
- 1736 Li XX, Britter RE, Koh TY, Norford LK, Liu CH, Entekhabi D, Leung DY (2010)
1737 Large-eddy simulation of flow and pollutant transport in urban street canyons with
1738 ground heating. *Boundary-Layer Meteorol* 137(2):187–204
- 1739 Lilly DK (1967) The representation of small-scale turbulence in numerical simula-
1740 tions. In: *Proc. IBM Scientific Computing Symposium on Environmental Sciences*,
1741 Yorktown Heights, New York, IBM form no. 320-1951, pp 195–209
- 1742 Lilly DK (1992) A proposed modification of the Germano subgrid-scale closure
1743 method. *Phys Fluids A* 4(3):633–635, DOI 10.1063/1.858280
- 1744 Lilly DK (2000) The meteorological development of large eddy simulation. In: RM K,
1745 Y K (eds) *IUTAM Symposium on Developments in Geophysical Turbulence. Fluid
1746 Mechanics and Its Applications*, vol 58, Springer, Dordrecht, chap 2, pp 5–18

- 1747 van der Linden SJ, Edwards JM, van Heerwaarden CC, Vignon E, Genthon C, Petenko
1748 I, Baas P, Jonker HJ, van de Wiel BJ (2019) Large-eddy simulations of the steady
1749 wintertime antarctic boundary layer. *Boundary-Layer Meteorol* 173(2):165–192
- 1750 Liu L, Coops NC, Aven NW, Pang Y (2017) Mapping urban tree species using inte-
1751 grated airborne hyperspectral and LiDAR remote sensing data. *Remote Sens Env-*
1752 *iron* 200:170–182
- 1753 Liu S, Meneveau C, Katz J (1994) On the properties of similarity subgrid-scale models
1754 as deduced from measurements in a turbulent jet. *J Fluid Mech* 275:83–119, DOI
1755 10.1017/S0022112094002296
- 1756 Lu H, Rutland CJ, Smith LM (2008) A posteriori tests of one-equation LES modeling
1757 of rotating turbulence. *Int J Mod Phys C* 19(12):1949–1964
- 1758 Macdonald R (2000) Modelling the mean velocity profile in the urban canopy layer.
1759 *Boundary-Layer Meteorol* 97(1):25–45
- 1760 Mahaffee WF, Stoll R (2016) The ebb and flow of airborne pathogens: Monitoring
1761 and use in disease management decisions. *Phytopathology* 106(5):420–431
- 1762 Mahrt L (1999) Stratified atmospheric boundary layers. *Boundary-Layer Meteorol*
1763 90(3):375–396
- 1764 Mahrt L, Thomas C (2016) Surface stress with non-stationary weak winds and stable
1765 stratification. *Boundary-Layer Meteorol* 159(1):3–21
- 1766 Margairaz F, Pardyjak ER, Calaf M (2020a) Surface thermal heterogeneities and the
1767 atmospheric boundary layer: The heterogeneity parameter. *Boundary-Layer Mete-*
1768 *orol* pp 1–27, DOI Accepted
- 1769 Margairaz F, Pardyjak ER, Calaf M (2020b) Surface thermal heterogeneities and the
1770 atmospheric boundary layer: The relevance of dispersive fluxes. *Boundary-Layer*
1771 *Meteorol* pp 1–27, DOI 10.1007/s10546-020-00509-w
- 1772 Maronga B, Raasch S (2013) Large-eddy simulations of surface heterogeneity ef-
1773 fects on the convective boundary layer during the LITFASS-2003 experiment.
1774 *Boundary-Layer Meteorol* 146(1):17–44
- 1775 Mason P, Callen N (1986) On the magnitude of the subgrid-scale eddy coefficient in
1776 large-eddy simulations of turbulent channel flow. *J Fluid Mech* 162:439–462
- 1777 Mason PJ (1989) Large-eddy simulation of the convective atmospheric boundary
1778 layer. *J Atmos Sci* 46(11):1492–1516
- 1779 Mason PJ, Derbyshire SH (1990) Large-eddy simulation of the stably-stratified
1780 atmospheric boundary layer. *Boundary-Layer Meteorol* 53:117–162, DOI
1781 10.1007/BF00122467
- 1782 Mason PJ, Thomson DJ (1992) Stochastic backscatter in large-eddy simulations of
1783 boundary layers. *J Fluid Mech* 242:51–78, DOI 10.1017/S0022112092002271
- 1784 Matheou G, Chung D (2014) Large-eddy simulation of stratified turbulence. part ii:
1785 Application of the stretched-vortex model to the atmospheric boundary layer. *J At-*
1786 *mos Sci* 71(12):4439–4460
- 1787 Mellado JP (2017) Cloud-top entrainment in stratocumulus clouds. *Annu Rev Fluid*
1788 *Mech* 49:145–169
- 1789 Mellor GL, Yamada T (1974) A hierarchy of turbulence closure models for planetary
1790 boundary layers. *J Atmos Sci* 31(7):1791–1806
- 1791 Meneveau C, Katz J (2000) Scale-invariance and turbulence models for large-eddy
1792 simulation. *Annu Rev Fluid Mech* 32(1):1–32, DOI 10.1146/annurev.fluid.32.1.1

- 1793 Meneveau C, Lund TS, Cabot WH (1996) A Lagrangian dynamic subgrid-scale model
1794 of turbulence. *J Fluid Mech* 319:353–385, DOI 10.1017/S0022112096007379
- 1795 Métais O (1998) Large-Eddy Simulations of Three-Dimensional Turbulent Flows:
1796 Geophysical Applications, Springer Netherlands, Dordrecht, pp 351–372
- 1797 Michioka T, Takimoto H, Sato A (2014) Large-eddy simulation of pollutant removal
1798 from a three-dimensional street canyon. *Boundary-Layer Meteorol* 150(2):259–275
- 1799 Miller NE, Stoll R (2013) Surface heterogeneity effects on regional-scale fluxes in the
1800 stable boundary layer: Aerodynamic roughness length transitions. *Boundary-Layer*
1801 *Meteorol* 149(2):277–301
- 1802 Mirocha J, Lundquist J, Kosović B (2010) Implementation of a nonlinear subfilter
1803 turbulence stress model for large-eddy simulation in the advanced research WRF
1804 model. *Mon Wea Rev* 138(11):4212–4228
- 1805 Mirocha JD, Kosović B (2010) A large-eddy simulation study of the influence of sub-
1806 sidence on the stably stratified atmospheric boundary layer. *Boundary-Layer Me-*
1807 *eteorol* 134(1):1
- 1808 Mittal R, Iaccarino G (2005) Immersed boundary methods. *Annu Rev Fluid Mech*
1809 37:239–261
- 1810 Moeng CH (1984) A large-eddy-simulation model for the study of planetary
1811 boundary-layer turbulence. *J Atmos Sci* 41(13):2052–2062, DOI 10.1175/1520-
1812 0469(1984)041<2052:ALES MF>2.0.CO;2
- 1813 Moeng CH, Sullivan PP (1994) A comparison of shear-and buoyancy-driven planetary
1814 boundary layer flows. *J Atmos Sci* 51(7):999–1022
- 1815 Moeng CH, Wyngaard JC (1988) Spectral analysis of large-eddy simulations of the
1816 convective boundary layer. *J Atmos Sci* 45(23):3573–3587
- 1817 Moeng CH, Wyngaard JC (1989) Evaluation of turbulent transport and dissipa-
1818 tion closures in second-order modeling. *J Atmos Sci* 46(14):2311–2330, DOI
1819 10.1175/1520-0469(1989)046<2311:EOTTAD>2.0.CO;2
- 1820 Moin P, Homsy G (2017) An appreciation of the life and work of William C.
1821 Reynolds (1933–2004). *Annu Rev Fluid Mech* 49(1):1–21, DOI 10.1146/annurev-
1822 fluid-122414-034434
- 1823 Moin P, Squires K, Cabot W, Lee S (1991) A dynamic subgrid-scale model for com-
1824 pressible turbulence and scalar transport. *Phys Fluids A* 3(11):2746–2757
- 1825 Monin A, Obukhov A (1954) Turbulent mixing in the atmospheric surface layer. *Tr*
1826 *Akad Nauk SSSR Geofiz Inst* 24(151):163–187
- 1827 Muñoz-EsTarza D, Kosović B, Mirocha J, van Beeck J (2014) Bridging the transition
1828 from mesoscale to microscale turbulence in numerical weather prediction models.
1829 *Boundary-Layer Meteorol* 153(3):409–440
- 1830 Nazarian N, Martilli A, Kleissl J (2018) Impacts of realistic urban heating, part
1831 i: Spatial variability of mean flow, turbulent exchange and pollutant dispersion.
1832 *Boundary-Layer Meteorol* 166(3):367–393
- 1833 Nieuwstadt F, Brost R (1986) The decay of convective turbulence. *J Atmos Sci*
1834 43(6):532–546
- 1835 Nieuwstadt FT (1984) The turbulent structure of the stable, nocturnal boundary layer.
1836 *J Atmos Sci* 41(14):2202–2216
- 1837 Nieuwstadt FT, Mason PJ, Moeng CH, Schumann U (1993) Large-eddy simulation of
1838 the convective boundary layer: A comparison of four computer codes. In: *Turbulent*

- 1839 Shear Flows 8, Springer, pp 343–367
- 1840 Niyogi D, Pyle P, Lei M, Arya SP, Kishtawal CM, Shepherd M, Chen F, Wolfe B
1841 (2011) Urban modification of thunderstorms: An observational storm climatology
1842 and model case study for the Indianapolis urban region. *J Appl Meteor Climatol*
1843 50(5):1129–1144
- 1844 Nugroho B, Hutchins N, Monty J (2013) Large-scale spanwise periodicity in
1845 a turbulent boundary layer induced by highly ordered and directional surface
1846 roughness. *International Journal of Heat and Fluid Flow* 41:90–102, DOI
1847 <https://doi.org/10.1016/j.ijheatfluidflow.2013.04.003>
- 1848 Pardyjak ER, Stoll R (2017) Improving measurement technology for the design of
1849 sustainable cities. *Meas Sci Technol* 28(9):092,001
- 1850 Patton EG, Shaw RH, Judd MJ, Raupach MR (1998) Large-eddy simulation of wind-
1851 break flow. *Boundary-Layer Meteorol* 87(2):275–307
- 1852 Patton EG, Sullivan PP, Moeng CH (2005) The influence of idealized heterogeneity
1853 on wet and dry planetary boundary layers coupled to the land surface. *J Atmos Sci*
1854 62(7):2078–2097
- 1855 Patton EG, Sullivan PP, Shaw RH, Finnigan JJ, Weil JC (2016) Atmospheric sta-
1856 bility influences on coupled boundary layer and canopy turbulence. *J Atmos Sci*
1857 73(4):1621–1647
- 1858 Peskin CS (1972) Flow patterns around heart valves: A numerical method. *J Comp*
1859 *Phys* 10(2):252–271, DOI [https://doi.org/10.1016/0021-9991\(72\)90065-4](https://doi.org/10.1016/0021-9991(72)90065-4)
- 1860 Philips D, Rossi R, Iaccarino G (2013) Large-eddy simulation of passive scalar dis-
1861 persion in an urban-like canopy. *J Fluid Mech* 723:404–428
- 1862 Pino D, Jonker HJ, De Arellano JVG, Dosio A (2006) Role of shear and the inversion
1863 strength during sunset turbulence over land: Characteristic length scales. *Boundary-*
1864 *Layer Meteorol* 121(3):537–556
- 1865 Piomelli U, Balaras E (2002) Wall-layer models for large-eddy simulation. *Annu Rev*
1866 *Fluid Mech* 34:349–374
- 1867 Piomelli U, Cabot WH, Moin P, Lee S (1991) Subgrid-scale backscatter in turbulent
1868 and transitional flows. *Phys Fluids A* 3(7):1766–1771, DOI 10.1063/1.857956
- 1869 Pope S (2000) *Turbulent Flows*. Cambridge University Press
- 1870 Pope SB (2004) Ten questions concerning the large-eddy simulation of turbulent
1871 flows. *New J Phys* 6:35–35, DOI 10.1088/1367-2630/6/1/035
- 1872 Porté-Agel F (2004) A scale-dependent dynamic model for scalar transport in large-
1873 eddy simulations of the atmospheric boundary layer. *Boundary-Layer Meteorol*
1874 112(1):81–105, DOI 10.1023/B:BOUN.0000020353.03398.20
- 1875 Porté-Agel F, Meneveau C, Parlange MB (2000) A scale-dependent dynamic model
1876 for large-eddy simulation: Application to a neutral atmospheric boundary layer. *J*
1877 *Fluid Mech* 415:261–284, DOI 10.1017/S0022112000008776
- 1878 Prandtl L (1925) 7. bericht über untersuchungen zur ausgebildeten turbulenz. *ZAMM*
1879 - *Journal of Applied Mathematics and Mechanics / Zeitschrift für Angewandte*
1880 *Mathematik und Mechanik* 5(2):136–139, DOI 10.1002/zamm.19250050212
- 1881 Raasch S, Harbusch G (2001) An analysis of secondary circulations and their ef-
1882 fects caused by small-scale surface inhomogeneities using large-eddy simulation.
1883 *Boundary-Layer Meteorol* 101(1):31–59

- 1884 Raasch S, Schröter M (2001) PALM—a large-eddy simulation model performing on
1885 massively parallel computers. *Meteorol Z* 10(5):363–372
- 1886 Rai RK, Berg LK, Kosović B, Haupt SE, Mirocha JD, Ennis BL, Draxl C (2019)
1887 Evaluation of the impact of horizontal grid spacing in terra incognita on cou-
1888 pled mesoscale–microscale simulations using the WRF framework. *Mon Wea Rev*
1889 147(3):1007–1027
- 1890 Randall DA, Shao Q, Moeng CH (1992) A second-order bulk boundary-layer model.
1891 *J Atmos Sci* 49(20):1903–1923
- 1892 Raupach M (1992) Drag and drag partition on rough surfaces. *Boundary-Layer Me-*
1893 *eteorol* 60(4):375–395
- 1894 Raupach M, Finnigan J, Brunet Y (1996) Coherent eddies and turbulence in vege-
1895 tation canopies: the mixing-layer analogy. In: *Boundary-layer Meteorology 25th*
1896 *Anniversary Volume, 1970–1995*, Springer, pp 351–382
- 1897 Richardson H, Basu S, Holtslag A (2013) Improving stable boundary-layer height
1898 estimation using a stability-dependent critical bulk Richardson number. *Boundary-*
1899 *Layer Meteorol* 148(1):93–109
- 1900 Sadique J, Yang XI, Meneveau C, Mittal R (2017) Aerodynamic properties of rough
1901 surfaces with high aspect-ratio roughness elements: Effect of aspect ratio and ar-
1902 rangements. *Boundary-Layer Meteorol* 163(2):203–224
- 1903 Sagaut P (2006) *Large Eddy Simulation for Incompressible flows: An Introduction*,
1904 3rd edn. Springer-Verlag, Berlin Heidelberg
- 1905 Saiki EM, Moeng CH, Sullivan PP (2000) Large-eddy simulation of the stably strati-
1906 fied planetary boundary layer. *Boundary-Layer Meteorol* 95(1):1–30
- 1907 Salesky ST, Anderson W (2018) Buoyancy effects on large-scale motions in convective
1908 atmospheric boundary layers: Implications for modulation of near-wall pro-
1909 cesses. *J Fluid Mech* 856:135–168
- 1910 Salesky ST, Chamecki M, Bou-Zeid E (2017) On the nature of the transition between
1911 roll and cellular organization in the convective boundary layer. *Boundary-Layer*
1912 *Meteorol* 163(1):41–68
- 1913 Sandström U, Van den Besselaar P (2018) Funding, evaluation, and the performance
1914 of national research systems. *Journal of Informetrics* 12(1):365–384
- 1915 Santos JM, Reis N, Castro I, Goulart EV, Xie ZT (2019) Using large-eddy simulation
1916 and wind-tunnel data to investigate peak-to-mean concentration ratios in an urban
1917 environment. *Boundary-Layer Meteorol* 172(3):333–350
- 1918 Schalkwijk J, Jonker HJ, Siebesma AP (2016) An investigation of the eddy-covariance
1919 flux imbalance in a year-long large-eddy simulation of the weather at Cabauw.
1920 *Boundary-Layer Meteorol* 160(1):17–39
- 1921 Schmidt H, Schumann U (1989) Coherent structure of the convective boundary layer
1922 derived from large-eddy simulations. *J Fluid Mech* 200:511–562
- 1923 Schumann U (1975) Subgrid scale model for finite difference simulations of tur-
1924 bulent flows in plane channels and annuli. *J Comp Phys* 18(4):376–404, DOI
1925 [https://doi.org/10.1016/0021-9991\(75\)90093-5](https://doi.org/10.1016/0021-9991(75)90093-5)
- 1926 Shao Y, Liu S, Schween JH, Crewell S (2013) Large-eddy atmosphere–land-surface
1927 modelling over heterogeneous surfaces: Model development and comparison with
1928 measurements. *Boundary-Layer Meteorol* 148(2):333–356

- 1929 Shaw RH, Patton EG (2003) Canopy element influences on resolved-and subgrid-
1930 scale energy within a large-eddy simulation. *Agric For Meteor* 115(1-2):5–17
- 1931 Shaw RH, Schumann U (1992) Large-eddy simulation of turbulent flow above and
1932 within a forest. *Boundary-Layer Meteorol* 61(1-2):47–64
- 1933 Shen S, Leclerc MY (1995) How large must surface inhomogeneities be before they
1934 influence the convective boundary layer structure? a case study. *Quart J Roy Meteor*
1935 *Soc* 121(526):1209–1228
- 1936 Shepherd MJ (2005) A review of current investigations of urban-induced rainfall and
1937 recommendations for the future. *Earth Interact* 9(12):1–27
- 1938 Shin HH, Dudhia J (2016) Evaluation of PBL parameterizations in WRF at subkilo-
1939 meter grid spacings: Turbulence statistics in the dry convective boundary layer.
1940 *Mon Wea Rev* 144(3):1161–1177, DOI 10.1175/MWR-D-15-0208.1
- 1941 Shin HH, Hong SY (2015) Representation of the subgrid-scale turbulent transport in
1942 convective boundary layers at gray-zone resolutions. *Mon Wea Rev* 143(1):250–
1943 271, DOI 10.1175/MWR-D-14-00116.1
- 1944 Siebesma AP, Soares PM, Teixeira J (2007) A combined eddy-diffusivity mass-flux
1945 approach for the convective boundary layer. *J Atmos Sci* 64(4):1230–1248
- 1946 Smagorinsky J (1963) General circulation experiments with the prim-
1947 itive equations. *Mon Wea Rev* 91:99–164, DOI 10.1175/1520-
1948 0493(1963)091<0099:gcewtp>2.3.co;2
- 1949 Sorbjan Z (1997) Decay of convective turbulence revisited. *Boundary-Layer Meteorol*
1950 82(3):503–517
- 1951 Sorbjan Z (2004) Large-eddy simulations of the baroclinic mixed layer. *Boundary-
1952 Layer Meteorol* 112(1):57–80
- 1953 Sorbjan Z (2007) A numerical study of daily transitions in the convective boundary
1954 layer. *Boundary-Layer Meteorol* 123(3):365–383
- 1955 Steeneveld G, Van de Wiel B, Holtslag A (2007) Diagnostic equations for the stable
1956 boundary layer height: Evaluation and dimensional analysis. *J Appl Meteor Clima-
1957 tol* 46(2):212–225
- 1958 Stevens B, Moeng CH, Ackerman AS, Bretherton CS, Chlond A, de Roode S, Ed-
1959 wards J, Golaz JC, Jiang H, Khairoutdinov M, Kirkpatrick MP, Lewellen DC,
1960 Lock A, Müller F, Stevens DE, Whelan E, Zhu P (2005) Evaluation of large-eddy
1961 simulations via observations of nocturnal marine stratocumulus. *Mon Wea Rev*
1962 133(6):1443–1462, DOI 10.1175/MWR2930.1
- 1963 Stoll R, Porté-Agel F (2006b) Effect of roughness on surface boundary conditions for
1964 large-eddy simulation. *Boundary-Layer Meteorol* 118(1):169–187
- 1965 Stoll R, Porté-Agel F (2008) Large-eddy simulation of the stable atmospheric bound-
1966 ary layer using dynamic models with different averaging schemes. *Boundary-Layer
1967 Meteorol* 126(1):1–28
- 1968 Stoll R, Porté-Agel F (2006a) Dynamic subgrid-scale models for momentum and
1969 scalar fluxes in large-eddy simulations of neutrally stratified atmospheric bound-
1970 ary layers over heterogeneous terrain. *Water Resour Res* 42(1):1–18, DOI
1971 10.1029/2005WR003989
- 1972 Su HB, Shaw RH, Paw KT, Moeng CH, Sullivan PP (1998) Turbulent statistics of
1973 neutrally stratified flow within and above a sparse forest from large-eddy simulation
1974 and field observations. *Boundary-Layer Meteorol* 88(3):363–397

- 1975 Sullivan PP, Patton EG (2011) The effect of mesh resolution on convective bound-
1976 ary layer statistics and structures generated by large-eddy simulation. *J Atmos Sci*
1977 68(10):2395–2415
- 1978 Sullivan PP, McWilliams JC, Moeng CH (1994) A subgrid-scale model for large-
1979 eddy simulation of planetary boundary-layer flows. *Boundary-Layer Meteorol*
1980 71(3):247–276
- 1981 Sullivan PP, Moeng CH, Stevens B, Lenschow DH, Mayor SD (1998) Structure of the
1982 entrainment zone capping the convective atmospheric boundary layer. *J Atmos Sci*
1983 55(19):3042–3064
- 1984 Sullivan PP, Weil JC, Patton EG, Jonker HJ, Mironov DV (2016) Turbulent winds and
1985 temperature fronts in large-eddy simulations of the stable atmospheric boundary
1986 layer. *J Atmos Sci* 73(4):1815–1840
- 1987 Sun J, Lenschow D, Burns S, Banta RM, Newsom R, Coulter R, Nappo CJ, Frasier
1988 S, Ince T, Balsley BB (2004) Atmospheric disturbances that generate intermittent
1989 turbulence in nocturnal boundary layers. *Boundary-Layer Meteorol* 110(2):255–
1990 279
- 1991 Svensson G, Holtslag AA (2009) Analysis of model results for the turning of the
1992 wind and related momentum fluxes in the stable boundary layer. *Boundary-Layer*
1993 *Meteorol* 132(2):261–277
- 1994 Teixeira J, Stevens B, Bretherton C, Cederwall R, Doyle JD, Golaz JC, Holtslag AA,
1995 Klein S, Lundquist JK, Randall DA, et al. (2008) Parameterization of the atmo-
1996 spheric boundary layer: a view from just above the inversion. *Bull Amer Meteor*
1997 *Soc* 89(4):453–458
- 1998 Tennekes H, Lumley J (1972) *A First Course in Turbulence*. MIT Press, Cambridge,
1999 MA
- 2000 Tomas J, Pourquie M, Jonker H (2016) Stable stratification effects on flow and pollu-
2001 tant dispersion in boundary layers entering a generic urban environment. *Boundary-*
2002 *Layer Meteorol* 159(2):221–239
- 2003 Tseng YH, Meneveau C, Parlange MB (2006) Modeling flow around bluff bodies
2004 and predicting urban dispersion using large eddy simulation. *Environ sci & tech*
2005 40(8):2653–2662
- 2006 Voller VR, Porté-Agel F (2002) Moore’s law and numerical modeling. *J Comp Phys*
2007 179(2):698–703
- 2008 Walko RL, Cotton WR, Pielke RA (1992) Large-eddy simulations of the effects of
2009 hilly terrain on the convective boundary layer. *Boundary-Layer Meteorol* 58(1-
2010 2):133–150, DOI 10.1007/BF00120755
- 2011 Walton A, Cheng A (2002) Large-eddy simulation of pollution dispersion in an urban
2012 street canyon—part ii: Idealised canyon simulation. *Atmos Environ* 36(22):3615–
2013 3627
- 2014 Watanabe T (2004) Large-eddy simulation of coherent turbulence structures associ-
2015 ated with scalar ramps over plant canopies. *Boundary-Layer Meteorol* 112(2):307–
2016 341
- 2017 Willingham D, Anderson W, Christensen KT, Barros J (2013) Turbulent boundary
2018 layer flow over transverse aerodynamic roughness transitions: Induced mixing and
2019 flow characterization. *Phys Fluids* 26:025,111–1–16

- 2020 Wilson J (1988) A second-order closure model for flow through vegetation. *Boundary-*
2021 *Layer Meteorol* 42(4):371–392
- 2022 Wong VC, Lilly DK (1994) A comparison of two dynamic subgrid closure methods for
2023 turbulent thermal convection. *Phys Fluids* 6(2):1016–1023, DOI 10.1063/1.868335
- 2024 Wood D (1981) The growth of the internal layer following a step change in surface
2025 roughness. Report TN – FM 57, Dept of Mech Eng, Univ of Newcastle, Australia
- 2026 Wyngaard J (2004) Toward numerical modeling in the “terra incognita”. *J Atmos Sci*
2027 61:1816–1826
- 2028 Wyngaard J (2010) *Turbulence in the atmosphere*. Cambridge University Press
- 2029 Wyngaard JC, Brost RA (1984) Top-down and bottom-up diffusion of a scalar in the
2030 convective boundary layer. *J Atmos Sci* 41(1):102–112
- 2031 Wyngaard JC, Weil JC (1991) Transport asymmetry in skewed turbulence. *Phys Fluids*
2032 A 3(1):155–162
- 2033 Xie Z, Castro IP (2006) LES and RANS for turbulent flow over arrays of wall-mounted
2034 obstacles. *Flow Turbul Combust* 76(3):291
- 2035 Xie ZT (2011) Modelling street-scale flow and dispersion in realistic winds—towards
2036 coupling with mesoscale meteorological models. *Boundary-Layer Meteorol*
2037 141(1):53–75
- 2038 Xie ZT, Castro IP (2009) Large-eddy simulation for flow and dispersion in urban
2039 streets. *Atmos Environ* 43(13):2174–2185
- 2040 Yaghoobian N, Kleissl J, et al. (2014) An improved three-dimensional simulation of
2041 the diurnally varying street-canyon flow. *Boundary-Layer Meteorol* 153(2):251–
2042 276
- 2043 Yamaguchi T, Randall DA (2012) Cooling of entrained parcels in a large-eddy simu-
2044 lation. *J Atmos Sci* 69(3):1118–1136
- 2045 Yan C, Huang WX, Miao SG, Cui GX, Zhang ZS (2017) Large-eddy simulation
2046 of flow over a vegetation-like canopy modelled as arrays of bluff-body elements.
2047 *Boundary-Layer Meteorol* 165(2):233–249
- 2048 Yang D, Shen L (2010) Direct-simulation-based study of turbulent flow over various
2049 waving boundaries. *J Fluid Mech* 650:131–180
- 2050 Yang J, Anderson W (2017) Numerical study of turbulent channel flow over sur-
2051 faces with variable spanwise heterogeneities: Topographically-driven secondary
2052 flows affect outer-layer similarity of turbulent length scales. *Flow Turbul Combust*
2053 100(1):1–17, DOI 10.1007/s10494-017-9839-5
- 2054 Yang X, Sadique J, Mittal R, Meneveau C (2015) Integral wall model for large eddy
2055 simulations of wall-bounded turbulent flows. *Phys Fluids* 27(2):025,112
- 2056 Yue W, Parlange MB, Meneveau C, Zhu W, Van Hout R, Katz J (2007) Large-eddy
2057 simulation of plant canopy flows using plant-scale representation. *Boundary-Layer*
2058 *Meteorol* 124(2):183–203
- 2059 Zhang R, Wang G, Guo S, Zamora ML, Ying Q, Lin Y, Wang W, Hu M, Wang Y
2060 (2015) Formation of urban fine particulate matter. *Chemical reviews* 115(10):3803–
2061 3855
- 2062 Zhu X, Iungo GV, Leonardi S, Anderson W (2017) Parametric study of urban-like
2063 topographic statistical moments relevant to a priori modelling of bulk aerodynamic
2064 parameters. *Boundary-Layer Meteorol* 162(2):231–253